Heaven's Light is Our Guide

RAJSHAHI UNIVERSITY OF ENGINEERING & TECHNOLOGY

RAJSHAHI-6204, BANGLADESH

Department of Materials Science and Engineering

A THESIS REPORT

ON

Synthesis and Characterization of Compositionally Complex Zinc Oxide $(Cu_xCo_xMn_xMg_xNi_x)Zn_{1-5x}O$ Thin Films by Spin Coating

Supervised by-

S.M. Nasim Rokon
Lecturer
Dept. of Materials Science & Engineering
RUET, Rajshahi-6204, Bangladesh.

Submitted by-

Israt Shukra
Roll No.: 1613015

Abu Shahid Ahmed
Roll No.: 1613022

Shafiul Alam
Roll No.: 1613030

November 2022

Heaven's Light is Our Guide

RAJSHAHI UNIVERSITY OF ENGINEERING & TECHNOLOGY

DEPARTMENT OF MATERIALS SCIENCE AND ENGINEERING

CERTIFICATE OF APPROVAL

The thesis work entitled "**Synthesis and Characterization of Compositionally Complex Zinc Oxide ($Cu_xCo_xMn_xMg_xNi_x)Zn_{1-5x}O$ Thin Films Obtained by Spin Coating**" submitted by Israt Shuqra, Roll No.: 1613015, Abu Shahid Ahmed, Roll No.: 1613022 and Shafiul Alam, Roll No.: 1613030 has been accepted as satisfactory in partial fulfillment of the requirements for the degree of Bachelor of Science in Materials Science and Engineering.

Signature of the External Examiner

_____

Dept. of Materials Science and Engineering

RUET, Rajshahi-6204, Bangladesh

Signature of the Supervisor

_____

S.M. Nasim Rokon

Lecturer

Dept. of Materials Science and Engineering

RUET, Rajshahi-6204, Bangladesh

Countersigned

_____

Dr. Mohammad Shahed Hasan Khan Tushar

Professor & Head

Dept. of Materials Science and Engineering

RUET, Rajshahi-6204, Bangladesh

Heaven's Light is Our Guide

RAJSHAHI UNIVERSITY OF ENGINEERING & TECHNOLOGY

DEPARTMENT OF MATERIALS SCIENCE AND ENGINEERING

A THESIS REPORT

ON

Synthesis and Characterization of Compositionally Complex Zinc Oxide $(Cu_xCo_xMn_xMg_xNi_x)Zn_{1-5x}O$ Thin Films Obtained by Spin Coating

This is to certify that the thesis work entitled "**Synthesis and Characterization of Compositionally Complex Zinc Oxide $(Cu_xCo_xMn_xMg_xNi_x)Zn_{1-5x}O$ Thin Films Obtained by Spin Coating**" is carried out by Israt Shuqra, Roll No.: 1613015, Abu Shahid Ahmed, Roll No.: 1613022 and Shafiul Alam, Roll No.: 1613030, under my supervision in the Department of Materials Science and Engineering of Rajshahi University of Engineering & Technology.

Signature of the Supervisor

_____

S.M. Nasim Rokon

Lecturer

Dept. of Materials Science and Engineering

RUET, Rajshahi-6204, Bangladesh

Signature of the Students

_____

Israt Shukra

Roll No.: 1613015

_____

Abu Shahid Ahmed

Roll No.: 1613022

_____

Shafiul Alam

Roll No.: 1613030

November, 2022

Approval page

The thesis titled "**Synthesis and Characterization of Compositionally Complex Zinc Oxide (CuxCoxMnxMgxNix)Zn1-5xO Thin Films Obtained by Spin Coating**" submitted by Israt Shuqra, Abu Shahid Ahmed, Shafiul Alam, Roll No: 1613015,1613022,1613030, Session:2016-2017 has been accepted as satisfactory in partial fulfillment of the requirement for the degree of Bachelor of Science in Materials Science & Engineering on November 2022.

_____

S.M. Nasim Rokon

Lecturer

Department of Materials Science and Engineering

RUET, Rajshahi-6204

Candidate's Declaration

We hereby declare that the undergraduate research work reported in this thesis has been performed by us under the supervision of Lecturer S.M. Nasim Rokon and this work has not been submitted elsewhere for any purpose.

Abu Shahid Ahmed

Student ID Number: 1613022

Department of Materials Science and Engineering

RUET, Rajshahi-6204

Israt Jahan Shukra

Student ID Number: 1613015

Department of Materials Science and Engineering

RUET, Rajshahi-6204

Shafiul Alam

Student ID Number: 1613030

Department of Materials Science and Engineering

RUET, Rajshahi-6204

Acknowledgement

First and foremost, we would like to express our gratitude to the Almighty Allah for His unwavering favor and countless blessings that allowed us to finish our research on schedule and without any obstacles.

We would like to take this opportunity to thank the following individual for his invaluable assistance provided while we were B.Sc. engineering students at the Department of Materials Science and Engineering at the Rajshahi University of Engineering and Technology (RUET).

We wish to express our sincere gratitude to Lecturer S.M. Nasim Rokon for providing us with all the necessary facilities, giving undivided attention and fostering us all the way through the research. His useful comments, remarks and engagement helped us with the learning process throughout the thesis.

Abstract

Due to their distinct structural traits and associated opportunities for modifying functional qualities, high-entropy alloys and oxides have recently had a greater impact on research communities. One way to compositionally create configurational disorder in a lattice structure is to change a single sublattice using a variety of different cations. The new structures of these kinds of metallic alloys and ceramic compounds are referred to as "high entropy stabilized structures." Based on this idea, we investigated the stability of ZnO wurtzite single phase structure using high level multielement (Co, Mn, Mg, Cu and Ni) doping with the aid of entropic contribution in this study. For this purpose thin films of pure ZnO and doped ($Cu_xCo_xMn_xMg_xNi_x$) $Zn_{1-x}O$ (where x=0.02, 0.04 and 0.06) were deposited through spin coationg technique. The fabricated undoped and doped films were entitled as Pure ZnO, CCZO10 (x=0.02), CCZO20 (x=0.04) and CCZO30 (x=0.06). To characterize the structural, morphological, optical and electrical properties of as-deposited films, X-ray diffraction (XRD), scanning electron microscopy (SEM), UV-Visible spectroscopy were conducted. The intricate structural characterization demonstrated the role of entropy in the highly doped CCZO30's single phase stabilization. The successful doping of five elements into ZnO with a small modification to the lattice characteristics was validated by XRD results. Doped films were found to have excellent optical properties, such as transmittance of around 82%, an increase in the energy band gap from 3.37 eV to 3.95 eV, and an improvement in optical conductivity, which merit great application potentials as TCOs and LED.

Keywords:

Compositionally complex Oxide, Spin coating, ZnO, (Cu, Co, Mn, Mg, Ni) doped

Table of Contents

List of Tables

List of Figures

Chapter 1

Introduction

1. Introduction

A thin film is a layer of material ranging from fractions of a nanometer (monolayer) to several micrometers in thickness. The semiconducting material, in thin film form are of particular interest because it has a various number of applications viz. transparent electrodes, photovoltaic devices, solar front panel display, surface acoustic wave devices, low emissivity coating for architectural glass, various gas sensors and heat reflectors for advanced gazing in solar cells [1]. Due to surface and interface effects; properties of thin film differ considerably from those of bulk and this will govern overall behavior of the thin films. Semiconductor physicists worldwide are constantly working on improving device efficiencies and realizing new and better devices by introducing new materials. One exciting group of materials is the functional oxides, of which zinc oxide (ZnO) is an important example. ZnO is relatively cheap, since both oxygen and zinc are elements the world possesses at a large scale. ZnO can be used as transparent conductive oxide (TCO) in solar cells, with the purpose of being the top electrode. The transparency of the material results in a larger area of the solar cell being exposed to light compared to thin metal contact fingers. Another common application of semiconductor materials is diodes. Light emitting diodes (LED) are sources of light used as traffic signals or the illumination source in TVs to name a few. ZnO has the potential of realizing blue LED and laser devices based on excitonic photon emission [2]. To release enhanced properties ZnO has already been explored as semiconducting thin films synthesizing by various routes and with various dopants [2]. Moreover, doped (single, co-doping and triple doping) ZnO based semiconducting thin films deposited by various techniques also synthesized successfully with its very high potentiality in the applications for numerous sectors. But till date, no attempt has been taken to analyze its performances by substituting the Zn sites with five dopants at a time. The significance behind the five elements doping is the rise of high entropy of mixing that stabilize the ZnO crystal structure to a high level of doping concentration. Entropic contributions to the stability of solids are very well understood and the mixing entropy has been used for forming various solids. Yeh et al reviewed a noble strategy of alloy design where a key concept of high entropy alloy formation was demonstrated [4]. In short, that can be summarized as; the configurational disorder is responsible for forming simple solid solutions and which are thoroughly studied for various applications especially due to their mechanical properties [5]. Many unexplored compositions and properties still remain for this class of materials due to their large phase space. In a recent report it has been shown that the configurational disorder can be used for stabilizing simple solid solutions of oxides, which should normally not form solid

solutions [6]. These new materials were called “entropy-stabilized oxides”. In this pioneering report, it was shown that after heating at high temperature and quenching, mixing five equimolar binary oxides yielded, an unexpected rock salt structure compound with statistical distribution of the cations in a face centered cubic lattice. Inheriting the concept of entropy stabilized oxides, the route of synthesizing entropic stabilization supported ZnO solid solution by doping the Zn^{2+} (rZn^{2+} =0.074 nm) sites with various sizes and valences of Cu^{2+}(r_{Cu2+}=0.073 nm), Co^{2+}(r_{Co2+}=0.072 nm), Mn^{2+}(r_{mn2+}=0.082 nm), Mg^{2+}(r_{Mg2+}=0.066 nm), and Ni^{2+}(r_{Ni2+}=0.078 nm) ions has been studied here. As in the previous work of high entropy generation with the mixture of five equimolar binary oxides; questions remain here whether ***high entropy will generate and stabilize the ZnO wurtzite crystal structure as the doping concentrations are 10% (in sample 01: $Cu_{.02}Co_{.02}Mn_{.02}Mg_{.02}Ni_{.02}Zn_{0.9}O$), 20% (in sample 02: $Cu_{.04}Co_{.04}Mn_{.04}Mg_{.04}Ni_{.04}Zn_{0.8}O$), 30% (in sample 03: $Cu_{.06}Co_{.06}Mn_{.06}Mg_{.06}Ni_{.06}Zn_{0.7}O$); not in equimolecular ratio as compared with Zn ion.*** Bearing in mind this probability whether the five dopants substituted ZnO single phase wurtzite structure will be obtained or not; we have forwarded to the synthesis of high entropy stabilized ZnO wurtzite structure thin films by low cost and manually operated spin coating technique. Interestingly, we found five element doped high entropy stabilized single phase wurtzite structured ZnO solid solution in thin films, as multi elements doping contributed high configurational disorder that may supported to stabilize the ZnO single phase. Thus, in this thesis work; synthesis of pure ZnO thin film and five cationic elements doped entropy stabilized ZnO thin films was carried out by spin coating method and subsequent characterizations of these thin films were conducted to evaluate their performances as TCO and LED. This thesis consists of total six chapters. In the Chapter 2, theory of crystalline materials, semiconductors and ZnO has been represented. This chapter also highlights the reviews of previous works and subsequently represents the sample characterization principles related to this topic. The next Chapter shows the detailed methodology of this study. In the results and discussion chapter, the obtained data in this study are presented with comprehensive discussions. In the conclusion chapter, summarized concluding remarks and suggestions for future works has been highlighted. Relevant references have been enlisted in Chapter 6.

Chapter II

Theory

2. Theory

The technology of thin film deposition has advanced dramatically during the past 30 years. This advancement was driven primarily by the need for new products and devices in the electronics and optical industries. The rapid progress in solid-state electronic devices would not have been possible without the development of new thin film deposition processes, improved film characteristics and superior film qualities. Thin film deposition technology is still undergoing rapid changes which will lead to even more complex and advanced electronic devices in the future.

2.1 Semiconductors

Semiconductor materials have electrical conductivities between metals and insulators and can be divided into two main groups; elemental semiconductors composed of a single element such as silicon, and compound semiconductors consisting of two or more elements such as zinc oxide [1]. The electrical conductivity of a semiconductor can be varied as a function of temperature and optical excitation intensity or by introducing impurities. These materials can be used in several applications since their electrical properties can be tailored to that application's specific needs. Typical applications for semiconductors are solar cells, transistors and diodes.

2.1.1 Energy band structure in solids

An isolated atom possesses several discrete energy levels, and some of these are filled with electrons. The energy levels which are either fully or partially filled, contains electrons called valence electrons. In solids, where the number of atoms is high (about Avogadro's number ~ 1023), the electron energy levels are no longer discrete. The large number of atoms bound together result in a periodic potential. A single electron's interaction with other electrons can be approximated by what is known as a nearly-free electron. However, in solids where the atoms remain in close proximity with one another, electrons are acted upon, or perturbed, by the electrons and nuclei of adjacent atoms. This influence is such that each distinct atomic state may split into a series of closely spaced electron states in the solid, to form what is termed an electron energy band [7]. The extent of splitting depends on interatomic separation and begins with the outermost electron shells, because they are the first to be perturbed as the atoms coalesce. Within each band, the energy states are discrete, yet the difference between adjacent states is exceedingly small. At the equilibrium spacing, band formation may not occur for the

electron subshells nearest the nucleus, as illustrated in Figure 2.1 (b). Furthermore, gaps may exist between adjacent bands, as also indicated in the figure; normally, energies lying within these band gaps are not available for electron occupancy. The conventional way of representing electron band structures in solids is shown in Figure 2.1 (a).

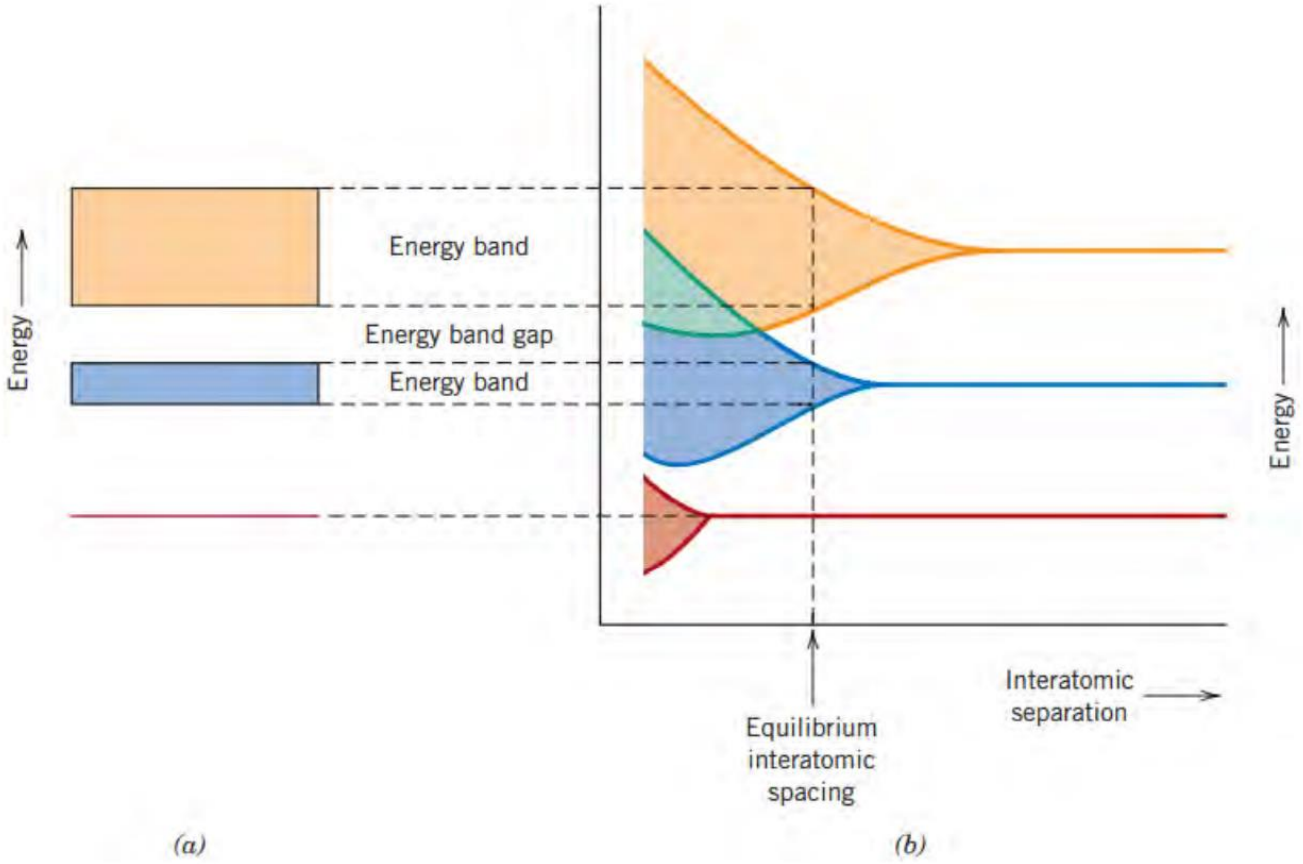

Figure 2.1: (a) The conventional representation of the electron energy band structure for a solid material at the equilibrium interatomic separation. (b) Electron energy versus interatomic separation for an aggregate of atoms, illustrating how the energy band structure at the equilibrium separation in (a) is generated. Reproduced from ref.[7].

The electrical properties of a solid material are a consequence of its electron band structure—that is, the arrangement of the outermost electron bands and the way in which they are filled with electrons. For obtaining electrical conductivity, electrons from the valence band must be excited to the conduction band, and the electrons (in CB) and holes in (VB) can move in an electric field. The magnitude of this gap distinguishes metals from semiconductors and semiconductors from insulators. Four different types of band structures are possible at 0 K. In the first (Figure 2.2 a), one outermost band is only partially filled with electrons. The energy corresponding to the highest filled state at 0 K is called the Fermi energy Ef, as indicated. This energy band structure is typified by some metals, in

particular those that have a single s valence electron (e.g., copper). Each copper atom has one 4s electron; however, for a solid composed of N atoms, the 4s band is capable of accommodating 2N electrons. Thus only half the available electron positions within this 4s band are filled. For the second band structure, also found in metals (Figure 2.2 b), there is an overlap of an empty band and a filled band. Magnesium has this band structure. At 0K all semiconductors are insulators. The main difference between semiconductors and insulators is that as the temperature is increased, the magnitude of the band gap of semiconductors allows electrons from the valence band to be excited to the conduction band. For insulators, the gap between the two bands is too large for excitation under normal circumstances, as seen in Figure 2.2 c, d

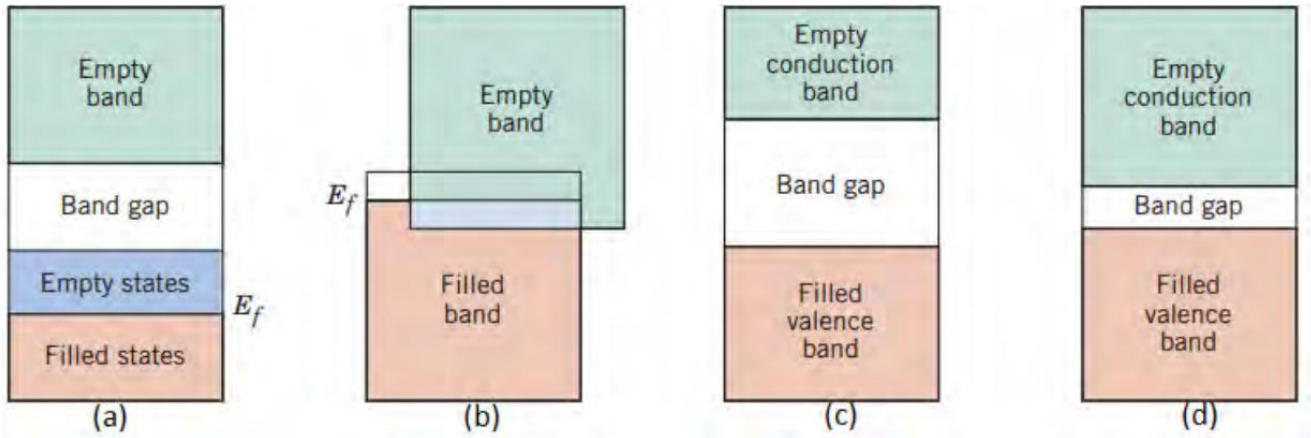

Figure 2.2: The various possible electron band structures in solids at 0 K. (a) For metals such as copper (b) For metals such as magnesium (c) Insulators and (d) Semiconductors. Reproduced from ref. [7].

2.1.2 Intrinsic and Extrinsic Semiconductors

A perfect semiconductor without dislocations, impurities or other defects is called an intrinsic semiconductor. Such a crystal is merely theoretical since it's practically impossible to fabricate. As there are no donors or acceptors in an intrinsic semiconductor, there are no electrons in CB at 0K. At higher temperatures, covalent bonds can be broken by exciting an electron to CB and leaving behind a missing electron in VB, or hole, making an electron-hole pair (EHP). The number of electrons in CB (n) must therefore be equal to the number of holes in VB (p) in an intrinsic material, i.e. n = p = ni (2.7) Where ni is the number of intrinsic charge carriers. A semiconductor containing impurities or lattice defects is termed an extrinsic semiconductor. The number of charge carriers can be tailored to a specific application by doping of the material. Doping the material is to introduce impurities as either donors or acceptors. Donors are atoms which have more valence electrons than the semiconductor

material. The excess electrons can be donated to the semiconductor and act as conduction electrons. Acceptors on the other hand are atoms with fewer valence electrons, and will therefore accept electrons from the crystal, and hence contribute with holes. Typically the number of introduced impurities is high and the number of electrons (with donor doping) will be so high that the number of holes can be neglected. This is called n-type doping. A p-type semiconductor is doped with a high amount of acceptors and the number of electrons can be neglected. Donors and acceptors have energy levels termed donor- and acceptor levels respectively, as shown in Figure 2.3 (a). If the energy of a donor level is in close proximity to the conduction band, which means that only a small amount of energy is needed to excite the donor electrons to the conduction band, it is called a shallow donor. If the donor level lies closer to the middle of the band gap it is called a deep donor. The same applies to acceptor levels but relative to the valence band. Electrons in VB can easily be excited to these states, leaving behind holes. At 0K any semiconductor, no matter how heavily doped, have no electrons in the conduction band. As the temperature is increased for an n-type semiconductor the donor atoms are ionized, i.e. the donor electrons are excited to the conduction band (the ionization part of Figure 2.3 b). Further temperature increase leads to all the donor electrons being excited to CB and the increase in electrons excited to CB is zero (the extrinsic region of Figure 2.3 b).

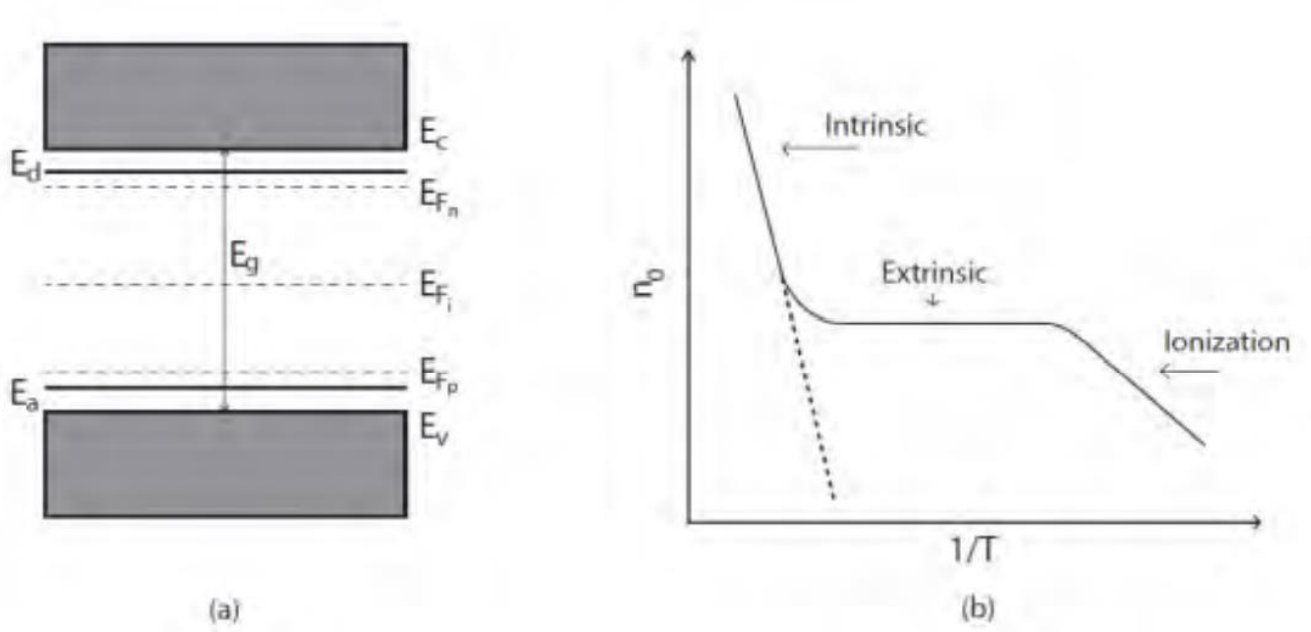

Figure 2.3: Band gap with donor level, E_d, in close proximity to the conduction band and acceptor level, E_a, close to the valence band (a). Figure (a) also shows the Fermi level (E_{Fi}) for an intrinsic semiconductor, and the Fermi levels, E_{Fn} and E_{Fp}, for n-type- and p-type semiconductors, respectively. Figure (b) shows the electron concentration in CB as a function of temperature, and which

mechanisms dominate. The dashed line shows the same function for an intrinsic semiconductor. Reproduced from ref. [8].

Finally the temperature is high enough to excite electrons from the valence band to the conduction band (the intrinsic region of Figure 2.3 b). The same holds for p-type semiconductors, but then electrons from the valence band are excited to the acceptor levels at relatively low temperatures, leaving holes behind.

2.1.3 Charge carriers in semiconductors

The concentration of electrons in the conduction band has several dependencies. The Fermi Dirac distribution function gives the probability of an energy state E being occupied by an electron at absolute temperature T;

$$f(E) = \frac{1}{1+e^{(E-E_F)/KT}} \ldots\ldots\ldots\ldots\ldots (2.1)$$

While the probability of finding an energy state occupied by a hole is equal to the probability of that energy state not being occupied by an electron;

$$1 - f(E) = 1 - \frac{1}{1+e^{(E-E_F)/KT}} \ldots\ldots\ldots\ldots\ldots\ldots (2.2)$$

E_F is the Fermi level of the semiconductor, k is the Boltzmann constant and T is the temperature. The Fermi level of a semiconductor is the dividing line between occupied and unoccupied states at absolute zero. For intrinsic semiconductors the Fermi level lies in the middle of the band gap, while for extrinsic semiconductors the Fermi level lies closer to the conduction- and valence band for n-type doping and p-type doping, respectively. The distribution function in equation (2.1) is plotted in Figure 2.4. From equation (2.1) it is clear that the probability of

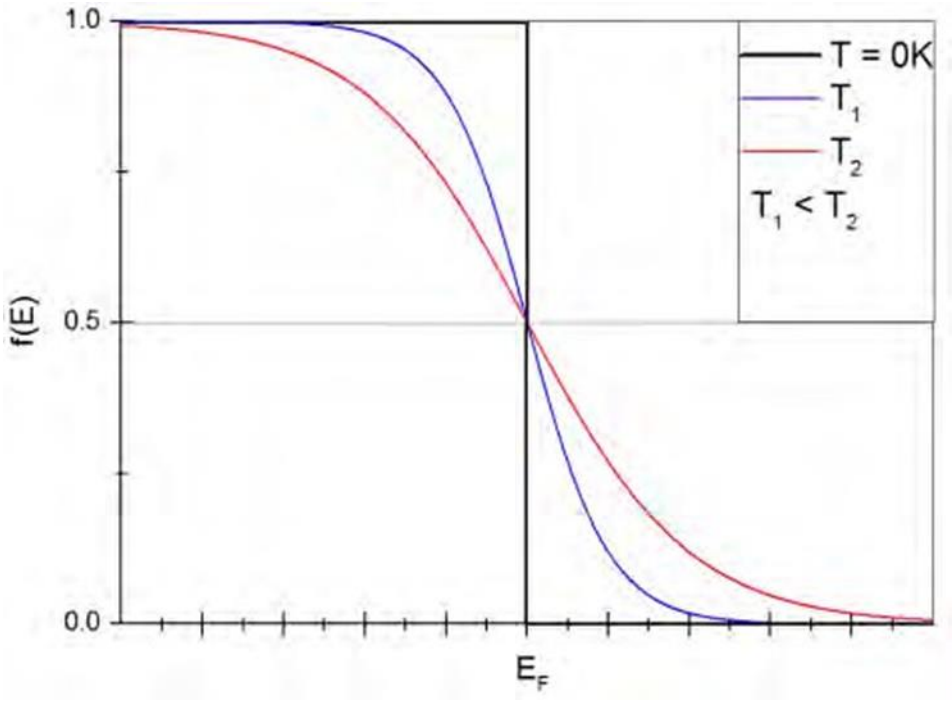

Figure 2. 4: The Fermi-Dirac distribution function. The black line shows the distribution at 0 K and the distribution is a step-function at the Fermi energy, whereas for T_1 (blue line) and T_2 (red line) which are temperatures higher than absolute zero, the distributions are more smeared out. Reproduced from ref.[9].

An energy state $E = E_F$ being occupied is 50% (irrespective of temperature). By examining the probability of the energy state $E = E_C$ being occupied, the concentration of electrons in CB and the hole concentration in VB can be found. At low energies, the Fermi-Dirac distribution is close to one and according to equation (2.2) the probability of finding a hole becomes very small. Hence the hole concentration decreases rapidly for energies lower than the top edge of VB.

2.2 Transparent Conducting Oxide

Transparent conducting oxides (TCOs) are both optically transparent and electrically conducting and, as such, are a critical component in almost all thin-film photovoltaic devices. TCOs are generally based on a limited class of metal oxide semiconductors such In_2O_3, ZnO and SnO_2, which are transparent due to their large band gap and can also tolerate very high electronic doping concentrations to yield conductivities of 1000 S/cm or higher [10]. TCO's consists of a group of materials that can be

thought of as ‘conjugate property materials’ in which one property, [in this case conductivity], is strongly coupled to a second property, namely, the extinction coefficient [11]. In this regard, it can be stated that materials like metals, that are highly conductive, will not normally transmit visible light, while highly transparent media like oxide glasses behave as insulators. The challenge for achieving materials that are both electrically conducting and optically transparent is to understand the fundamental material structure/property relationships that control these properties so that they may be decoupled such that the material retains transparency while becoming electrically conductive. To an extent, many phenomenological approaches based upon well understood physical principles have been reported to achieve materials having these properties. More recent studies push the envelope of the earlier work through understanding, at a fundamental level, the microscopic nature of the conductivity process in order to discover the role of chemical structure, bonding, and film morphology on charge transport. For most optoelectronic devices especially the ones with flat panel displays, it is essential to have a transparent electrode with TCO. Although tin-doped indium oxide (commonly called indium-tin oxide, or ITO) thin films deposited using magnetron sputtering have been in practical use for most of the transparent electrode applications, there are many reports on other TCO’s as well as deposition methods [12,13]. A stable supply of ITO for the fast-expanding market for optoelectronic devices may be difficult because of the cost and scarcity of indium, the principal material of ITO. In addition, recent developments in optoelectronic devices require thin-film transparent electrodes with specialized properties. Recent research on materials and techniques for making TCO’s is mainly focused on resolving these problems. For example, there are several research groups working all over the world aiming at the modification of zinc oxide (ZnO) as an alternative to costly ITO [14, 15].

2.2.1 General properties of TCO:

TCOs are unique materials that combine optical transparency (band gaps > 3.1 eV) and electrical conductivity (carrier concentration of at least 1019cm-3). Band gap > 3.1 eV ensures that visible light photons cannot excite electrons from the valence band (VB) to the conduction band (CB). These transparent materials are thus made electrically conducting by the introduction of defects, [intrinsic or extrinsic] into the system. TCOs can be classified as n-type or p-type, according to the defects and type of conduction of the material. These defects form split off acceptor (unoccupied) levels above the valence band maximum (VBM) in the case of p-type conduction, and donor (occupied) levels below the conduction band minimum (CBM) in the case of n-type conduction. ZnO based TCO films have been prepared through various kinds of methods [16]

and each of them has its own advantages and drawbacks. Even if the films are prepared by the same method, thickness, substrate, growth temperature, dopant, and their content will play a crucial role in structural, electrical, and optical properties of films. Therefore, whether we can optimize the fabrication of high-quality doped zinc oxide thin films at low cost determines the future of ZnO-based TCO films.

2.2.1.1 Electrical conductivity:

TCOs are wide band gap (E_g) semiconducting oxides, with conductivity in the range 10^2 to 1.2×10^6 (S), which is due to doping either by oxygen vacancies or by extrinsic dopants. In the absence of doping, these oxides become very good insulators, with resistivity > 10^{10} Ohm-cm. Most of the TCOs are n-type semiconductors. Electrical conductivity of n-type TCO thin films depends on the electron density in the conduction band and on their mobility. To explain the TCO characteristics, various population mechanisms and several models describing the electron mobility were proposed. Some characteristics of the mobility and the processes by which the conduction band is populated with electrons were shown to be interconnected by electronic structure studies [17]. For example, the mobility is proportional to the magnitude of the band gap. Further doping of elements with more charge carriers can increase conductivity of these TCOs. Higher doping concentration reduces carrier mobility to a degree so that the conductivity cannot be increased. Moreover it decreases the optical transmission at the near infrared edge. With the increase in dopant concentration, the resistivity reaches a lower limit, beyond which it cannot decrease. But the optical window becomes narrower.

2.2.1.1 Optical properties:

As mentioned above, besides high conductivity good TCO thin films should have very low absorption coefficient in the near UV-VIS-NIR region. Transmission in the near- UV region is limited by Eg as photons with energy larger than Eg are absorbed. However, there are no “ideal” TCOs thin films, and even if such films could be deposited, reflection and interference would also affect the transmission. Hence, 100% transparency over a wide region cannot be obtained.

2.2.1.2 Work function:

Energy difference between Fermi energy level and vacuum level corresponds to the work

function (f) which is the minimum amount of energy needed to remove an electron from the metal. In metals, work function and ionization energy are the same. Condition of the surface can strongly affect the work function. Presence of minute quantity of contamination (less than a monolayer of atoms or molecules), or the occurrence of surface reactions (oxidation or similar) can change the work function substantially. Changes of the order of 1 eV are common for metals and semiconductors, depending on the surface condition. These changes are due to the formation of electric dipoles at the surface, which change the energy an electron needs to leave the sample. Due to the sensitivity of the work function to chemical changes on surfaces, its measurement can give valuable insight into the condition of a given surface [18]. In a nondegenerate semiconductor (having a moderate doping level), the Fermi level is located within the band gap. This means that work function is now different from the ionization energy (energy difference between valence bands maximum (VBM) and vacuum level). In a semiconductor, the Fermi level becomes a somewhat theoretical parameter since there are no allowed electronic states within the band gap. This means that Fermi distribution needs to be considered, which is a statistical function that gives the probability to find an electron in a given electronic state. Fermi level refers to the point on the energy scale where the probability is just 50%. Work function of untreated AZO and ITO is generally equated at ~ 4.97 and 4.7eV respectively [19], where the plasma cleaning of the TCO in O_2 generally increased the work function by about 0.1 - 0.3 eV.

2.2.1.3 Thermal and Chemicalstability:

Thermal stability temperature is a threshold temperature, above which TCO films show appreciable change or degradation in its properties. The reported thermal stability temperatures for ZnO, SnO_2 and Cd_2SnO_4 are 250°C, 500°C and 700°C, respectively [20]. Above these temperatures, chemical decompositions of the films occur, which degrade the quality of the films. Many commercial substrates are temperature sensitive (glass < 500°C, polymer <200°C) and hence, restrict the processing temperature. Moreover, observations of chemical reaction of the TCO films with the substrate and the subsequent layers have been reported in the literature [21]. Thermal stability is essential for the developed TCOs from the application point of view as these TCOs may be exposed to various extreme environments. Chemical stability of a TCO is determined by its ability to resist corrosive environment and treatment. For applications such as amorphous Si solar cells, sensitivity of TCO to reducing atmospheres is an important concern. ITO undergoes heavy reduction when exposed to hydrogen environments. Comparatively, doped ZnO films are much more stable in reducing atmospheres and plasmas containing hydrogen species [20]. Therefore, ZnO based TCOs may be preferred for the applications involving hydrogen plasma processing. In contrast, for oxidizing atmospheres, especially at high temperatures, ITO shows better stability compared to other TCOs.

2.2.2 ZnO as TCOs

A *transparent conductive oxide* (TCO) can act as the top electrode of a solar cell. For a TCO to be efficient as an electrode (front and back), the material must possess some crucial properties; the resistivity should be as low as possible, meanwhile the carrier concentration is reduced to reduce unwanted free carrier absorption in the infra-red range. The mobility of the carriers on the other hand should be as large as possible, to increase the TCOs conductivity, while at the same time keeping the absorption coefficient low [22]. Park et. al. [23] deposited Ga-doped ZnO on quartz substrates using pulsed laser deposition. A resistivity of 8.12×10^{-5} Ωcm and a visible transmittance of above 90% were obtained for sample deposited at 300°C. A significant reduction in resistivity value with high transparency released from the report of ZnO/Ag composite thin film structure conducted by Shau et al. [24, 25]. The group fabricated ZnO/Ag thin film/ZnO multilayer sandwich-like structures such as those shown in scheme Figure 2.5.

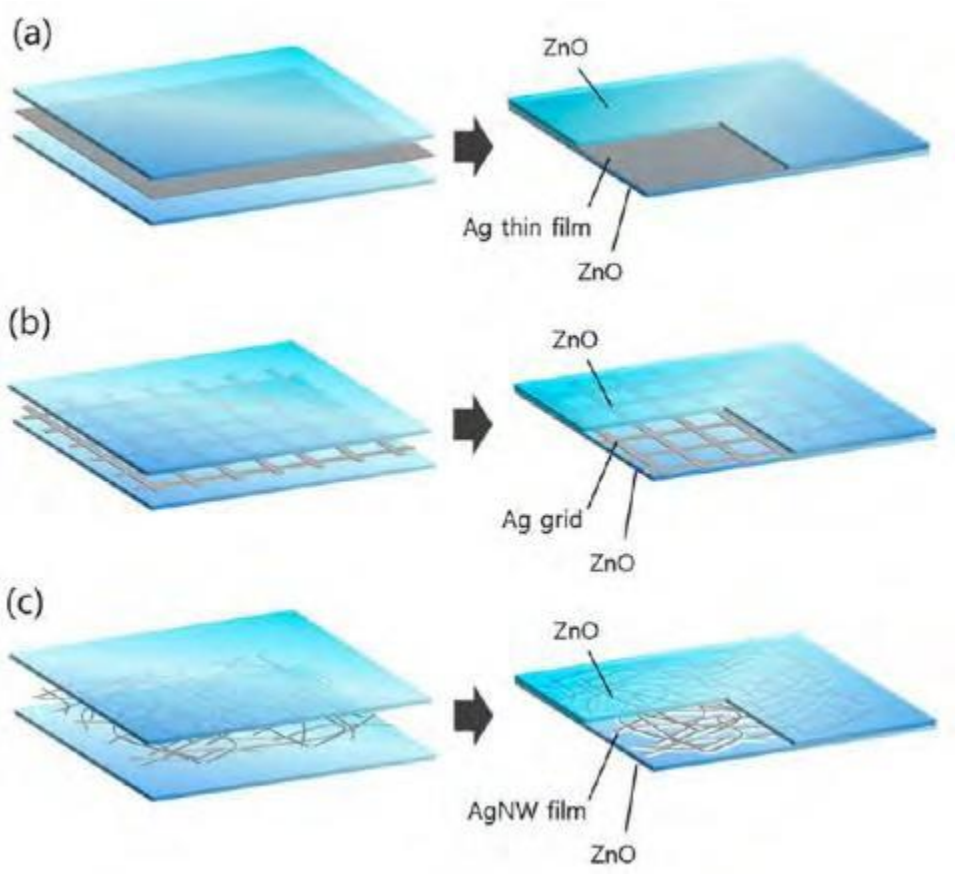

Figure 2.5: Schematics of (a) ZnO/ Ag film/ZnO structure with an Ag thin film layer between two transparent ZnO layers. (b) ZnO/Ag grid/ZnO structure in which the Ag grid is inserted. (c) ZnO/AgNW/ZnO structure in which an Ag nanowire network is present instead of an Ag thin film. Reproduced from ref. [24].

The insertion of an ultrathin silver film with the lowest resistivity ($1.6*10^{-6}$ Ω-cm) can dramatically lower the sheet resistance, while the thin film at the nanometer scale can transmit visible light [26].

2.3 LED

A *light emitting diode* (LED) is a p-n junction (in which p-type material brought together with an n-type material) where the current is injected in forward bias. The electrons on the n-side and holes on the p-side will then diffuse to the opposite side, leaving behind uncompensated donors and acceptors, respectively. As more carriers diffuse, an electric field will be built up in the transition (depletion) region, preventing further diffusion. Band bending occurs in order to keep

the Fermi level constant throughout the device, and the potential difference between the n- and p- side is called the contact potential. When the junction is in equilibrium, the carrier diffusion due to the concentration gradient and the carrier drift due to the electrical field in the transition region cancel each other out, resulting in no net current. Current is passed through the device in forward bias, and e^- and h^+ recombinations occur within the neutral (depletion) region of the p-n junction. When excited electrons and holes recombine in a direct band gap semiconductor, the energy is released by emitting photons. The emitted light will have the color corresponding to the band gap energy [27]. Since electrons and holes form tightly bound excitons in ZnO, near-band gap recombinations are efficient at room temperature, and ZnO is highly suited for LED devices [28]. ZnO nanostructure exhibits very active optical properties. The photoluminescence (PL) spectra of ZnO shows stronger UV emission and dry low emission in the visible region which is associated with the defect states present in the nanostructures. When transitions occur through defect states, light emission takes place in the visible region and transitions from different defect states results in emission at different wavelengths. There are reports on the green, red and blue[30] emission in ZnO films. However, the intensity of emission should be very strong to consider them for the device applications. The strong emission can be achieved by doping ZnO host lattice with external dopants. Shi et al. [31] have reported the enhancement of blue luminescence in ZnO thin films by doping rare earth element Ce. However, due to their less availability, doping rare earth materials would become costlier. S. Chawla et al. [32] have reported the possible application of ZnO thin film in white light generation by Mg doping.

2.4 ZnO

2.4.1 Crystal Structure of ZnO

ZnO is a II-VI semiconductor compound, with wurtzite as the thermodynamically stable phase at ambient conditions. ZnO has a hexagonal unit cell with the lattice parameters a = b = 3.2495 (± 0.00002) Å and c = 5.2069 (± 0.0001) Å as determined by Heller et al. [33], and belongs to the space group P63mc as seen in Figure 2.6. Wurtzite structure has hexagonal unit cell with two lattice parameters “a” and “c” in the ratio of c/a=1.66. The structure is composed of two interpenetrating hexagonal-close-packed (hcp) sub lattices, each of which consists of one type atom displaced with respect to each other along the three fold c-axis by the amount of u=3/8=0.375 (in ideal wurtzite structure) in fractional coordinate (the u parameter is defined as length of the bond parallel to the c axis, in unit of c). Each sub lattice includes four atoms per unit cell and every atom of one kind (group-II atom) is surrounded by four atoms of the other kind (group-VI) or vice versa, which are coordinated at the edges of a tetrahedron. These tetrahedrons are generally of sp3 covalent bonding, but these materials also have substantial ionic character that tends to increase the band gap beyond the one expected from the covalent bonding. In real ZnO crystal, the wurtzite structure deviates from the ideal arrangement, by changing the c/a ratio. The structure consists of alternating bi-atomic (0001) planes with a stacking sequence of AaBbAaBb⋯ [34].

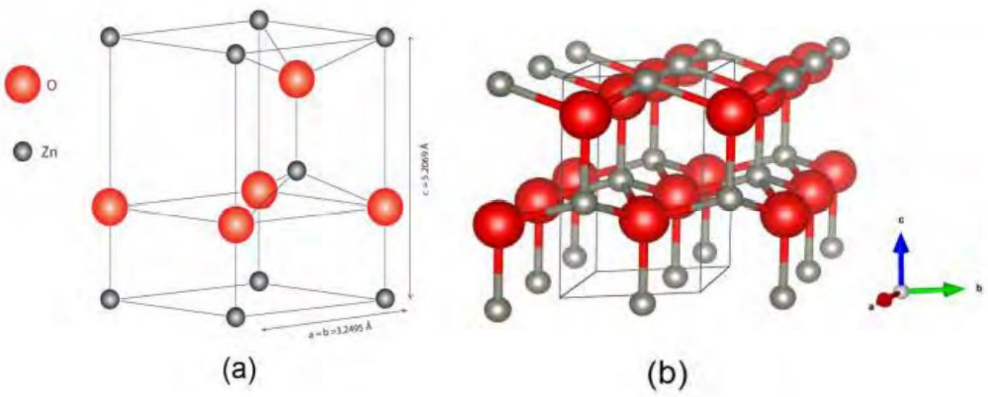

Figure 2.6: Illustration of wurtzite ZnO in its hexagonal unit cell (a) and more atoms added to illustrate the alternating biatomic planes (b). The cell parameters are a = b = 3.2495 Å and c = 5.2069 Å. Figure (b) was created using the VESTA software [35].

The positive z direction for the crystal is the [0001] axis which points from the face of the oxygen plane to the zinc plane. Bonds along the c direction going from an zinc cation to an oxygen anion has a Zn polarity, and the opposite is true for bonding from oxygen to zinc and the two sides of the crystal is called Zn-face [0001] and O-face [000$\bar{1}$].

2.4.2 Defects in ZnO

The control of defects and associated charge carriers is of paramount importance in applications that exploit the wide range of properties of doped ZnO. However, Solid surfaces contain segregated impurities, adsorbed gases that act as sources and sinks of electrons, and associated space charge regions. In nanostructured ZnO (as well as in other materials), the small length scales and large surface-to-volume ratio mean that surface defects play a stronger role in controlling properties. It is also critically important to understand defects in ZnO doped with aliovalent ions, either purposefully for achieving certain functionality or through accidental doping during the growth process. There are a number of intrinsic defects with different ionization energies. The Kröger Vink notation uses: i = interstitial site, Zn = zinc, O = oxygen, and V = vacancy. The terms indicate the atomic sites, and superscripted terms indicate charges, where a dot indicates positive charge, a prime indicates negative charge, and a cross indicates zero charge, with the charges in proportion to the number of symbols. Fig. 2.7 shows that there are a number of defect states within the bandgap of ZnO. The donor defects are: Zni •• , Zni• , Zni*, VO •• , VO • , VO and the acceptor defects are: VZn", VZn' [36].

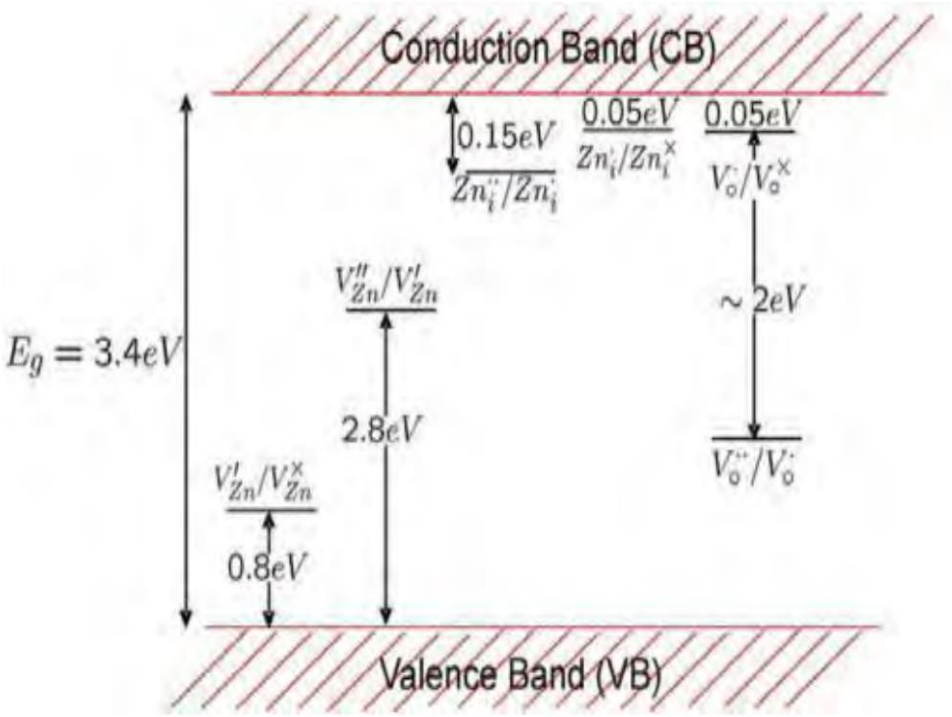

Figure 2.7: Energy levels of native defects in ZnO. Reproduced from ref. [36].

The defect ionization energies vary from ~0.05-2.8 eV [37]. Zn interstitials and oxygen vacancies are known to be the predominant ionic defect types. However, which defect dominates in native, undoped ZnO is still a matter of great controversy.

2.4.3 n type ZnO

ZnO with a wurtzite structure is naturally an n-type semiconductor because of a deviation from stoichiometry due to the presence of intrinsic defects such as O vacancies VO and Zn interstitials Zni. Undoped ZnO shows intrinsic n-type conductivity with very high electron densities of about 1021 cm−3.400 Although it is experimentally known that unintentionally doped ZnO is n type, whether the donors are Zni and VO is still controversial. n-type doping is performed in ZnO by group-III elements Al, Ga, and In as substitutional elements for Zn [38] and group-VII elements Cl and I as substitutional elements for O can be used as n-type dopants [39]. Doping with Al, Ga, and In has been attempted by many groups, resulting in high-quality, highly conductive n-type

ZnO films. Such films are successfully used in various applications as n-type layers in light emitting diodes as well as transparent Ohmic contacts.

2.5 Thin Film Deposition Techniques

Deposition technology can well be regarded as the major key to the creation of devices such as computers, since microelectronic solid-state devices are all based on material structures created by thin-film deposition. Electronic engineers have continuously demanded films of improved quality and sophistication for solid-state devices, requiring a rapid evolution of deposition technology. Equipment manufacturers have made successful efforts to meet the requirements for improved and more economical deposition systems and for in situ process monitors and controls for measuring film parameters. Another important reason for the rapid growth of deposition technology is the improved understanding of the physics and chemistry of films, surfaces, interfaces, and microstructures made possible by the remarkable advances in analytical instrumentation during the past twenty years. A better fundamental understanding of materials leads to expanded applications and new designs of devices that incorporate these materials. Thin films are defined as coatings of a thickness from about 5 Angstroms (Å) to a few micrometers (μm) [40]. Several materials may be deposited as thin films on passive substrates such as glass or ceramic or on active substrates such as silicon. The act of applying a thin film to a surface is known as thin-film deposition. Thin film deposition is a technique for depositing a thin film of material onto a substrate or onto previously deposited layers. "Thin" is a relative term, but most deposition techniques allow layer thickness to be controlled within a few tens of nanometers, and some (molecular beam epitaxy) allow single layers of atoms to be deposited at a time. It is useful in the manufacture of optics (for reflective or anti-reflective coatings, for instance), electronics (layers of insulators, semiconductors, and conductors form integrated circuits), packaging (i.e., aluminum-coated PET film) and in contemporary art. Similar processes are sometimes used where thickness is not important: for instance, the purification of copper by electroplating and the deposition of silicon and enriched uranium by a CVD-like process after gas-phase processing.

Deposition techniques fall into two broad categories:

i) Chemical Techniques

ii) ii) Physical Techniques

(i)Chemical Techniques

These processes exploit the creation of solid materials directly from chemical reactions in gas and/or liquid compositions or with the substrate material. The solid material is usually not the only product formed by the reaction. Byproducts can include gases, liquids and even other solids. Thin films from chemical deposition techniques tend to be conformal, rather than directional.

Depositions that happen because of a chemical reaction are as follows:

• Chemical Vapor Deposition (CVD)

• Electrodeposition

• Epitaxy

• Thermal oxidation

(ii) Physical Techniques Physical deposition uses mechanical or thermodynamic means to produce a thin film of solid. Common for all these processes are that the material deposited is physically moved on to the substrate. In other words, there is no chemical reaction which forms the material on the substrate. This is not completely correct for casting processes, though it is more convenient to think of them that way. This is by no means an exhaustive list since technologies evolve continuously. Depositions that happen because of a physical reaction:

• Physical Vapor Deposition (PVD)

• Casting

The classification of the different deposition processes is illustrated in the Figure 2.8:

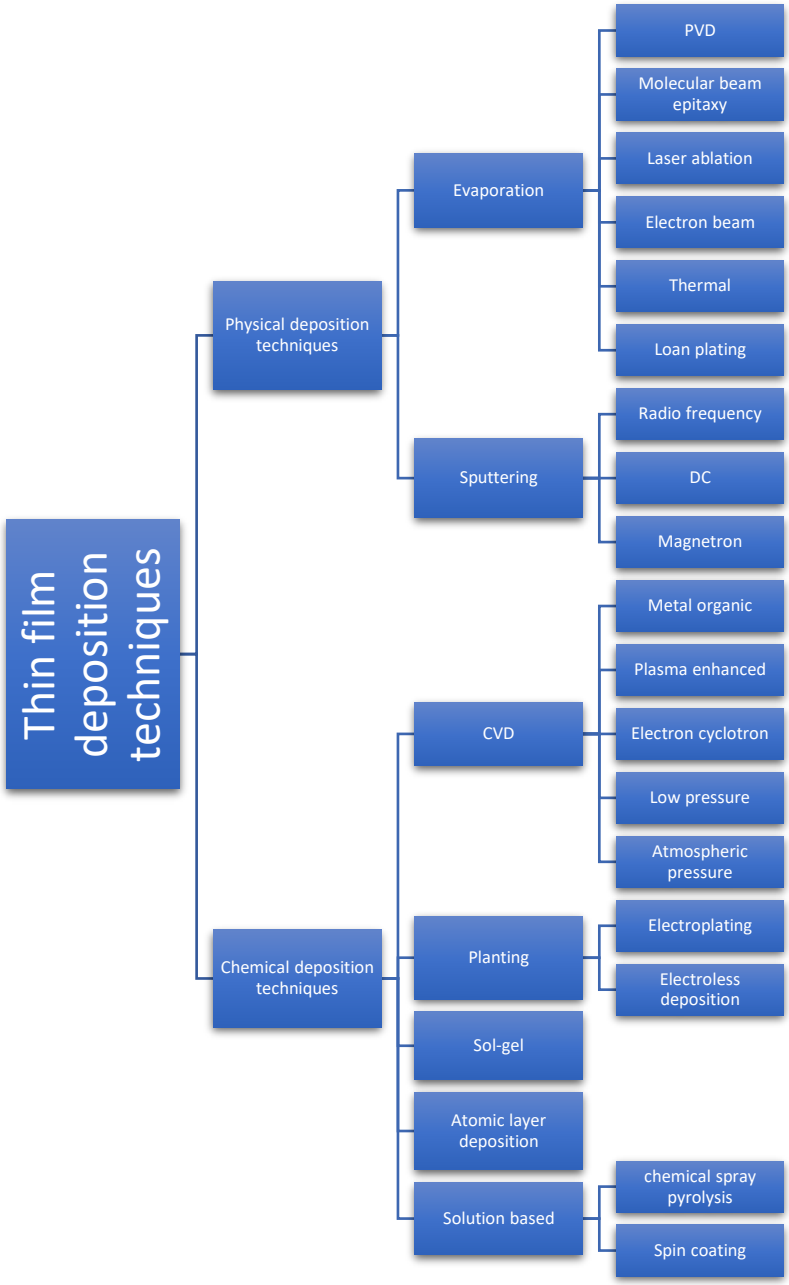

Figure 2.8: Classification of different film deposition techniques. Reproduced from ref. [41]

2.6 Overview of sol gel process:

In materials science, the sol-gel process is a method for producing solid materials from small molecules shown in figure 2.9. The method is used for the fabrication of metal oxides. The process involves conversion of monomers into a colloidal solution (*sol*) that acts as the precursor for an integrated network (or *gel*) of either discrete particles or network polymers. Typical precursors are metal alkoxides.

In the processing of fine ceramics, the irregular particle sizes and shapes in a typical powder often lead to non-uniform packing morphologies that result in packing density variations in the powder compact. Uncontrolled flocculation of powders due to attractive van der Waals forces can also give rise to microstructural inhomogeneities. Differential stresses that develop as a result of non- uniform drying shrinkage are directly related to the rate at which the solvent can be removed, and thus highly dependent upon the distribution of porosity. Such stresses have been associated with a plastic-to-brittle transition in consolidated bodies and can yield to crack propagation in the unfired body if not relieved. In addition, any fluctuations in packing density in the compact as it is prepared for the kiln are often amplified during the sintering process, yielding inhomogeneous densification. Some pores and other structural defects associated with density variations have been shown to play a detrimental role in the sintering process by growing and thus limiting end-point densities. Differential stresses arising from inhomogeneous densification have also been shown to result in the propagation of internal cracks, thus becoming the strength controlling flaws.

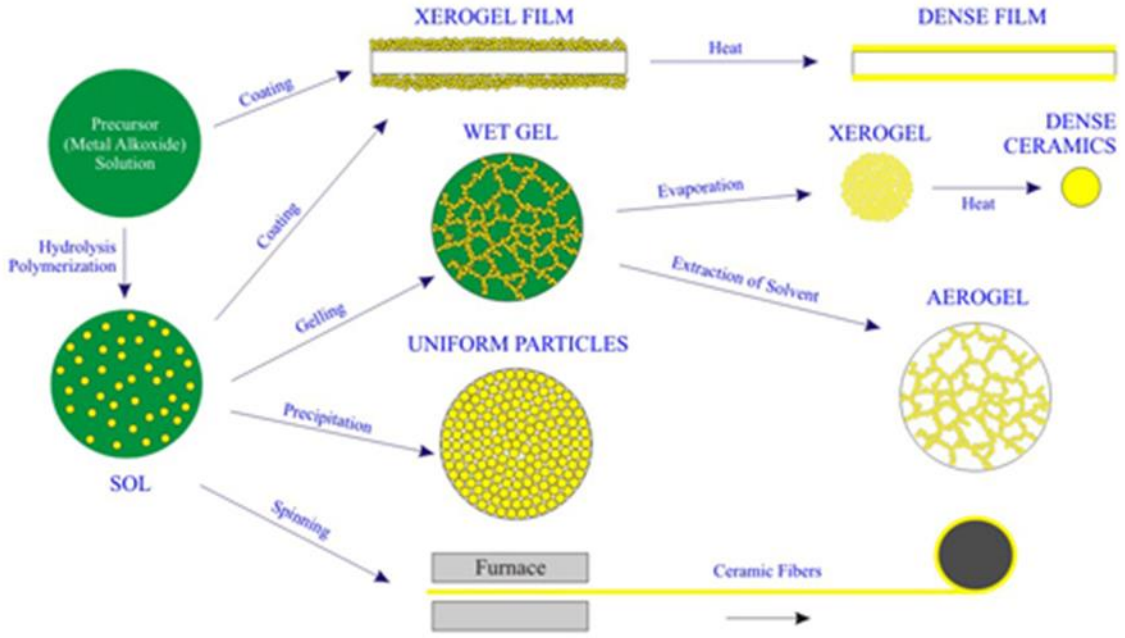

Figure 2.9 Basics of synthesis by sol gel methodology

It would therefore appear desirable to process a material in such a way that it is physically uniform with regard to the distribution of components and porosity, rather than using particle size distributions which will maximize the green density. The containment of a uniformly dispersed assembly of strongly interacting particles in suspension requires total control over particle-particle interactions. Monodisperse colloids provide this potential.

Monodisperse powders of colloidal silica, for example, may therefore be stabilized sufficiently to ensure a high degree of order in the colloidal crystal or polycrystalline colloidal solid which results from aggregation. The degree of order appears to be limited by the time and space allowed for longer-range correlations to be established. Such defective polycrystalline structures would appear to be the basic elements of nanoscale materials science, and, therefore, provide the first step in developing a more rigorous understanding of the mechanisms involved in microstructural evolution in inorganic systems such as sintered ceramic nanomaterials.

The applications for sol gel-derived products are numerous. For example, scientists have used it to produce the world's lightest materials and also some of its toughest ceramics. One of the

largest application areas is thin films, which can be produced on a piece of substrate by spin coating or dip coating. Protective and decorative coatings and electro-optic components can be applied to glass, metal and other types of substrates with these methods. Cast into a mold, and with further drying and heat-treatment, dense ceramic or glass articles with novel properties can be formed that cannot be created by any other method. Other coating methods include spraying, electrophoresis, inkjet printing or roll coating.

2.6.1. Sol gel coating technique:

The sol-gel process is a low-temperature process that uses inorganic or metal organic precursors to produce metal oxide molecules in solution form. The solution is synthesized based on the hydrolysis and condensation reactions of organometallic compounds in alcohol-based solutions. Several methods can then be used to deposit CCZO films using the solutions, one of which is spin coating, will be discussed below.

Spin-Coating for this technique, the material to be deposited is dissolved or dispersed into a solvent, and this coating solution is then deposited onto the substrate surface and spun off to leave a uniform layer of thin film on the substrate. As shown in Figure 2.10, the four key phases in the spin-coating process are:

1. Deposition of solution onto the substrate.
2. Spreading of solution from center of substrate to the sides (spin-up).
3. Gradual thinning of solution (spin-off).
4. Gelation due to solvent evaporation.

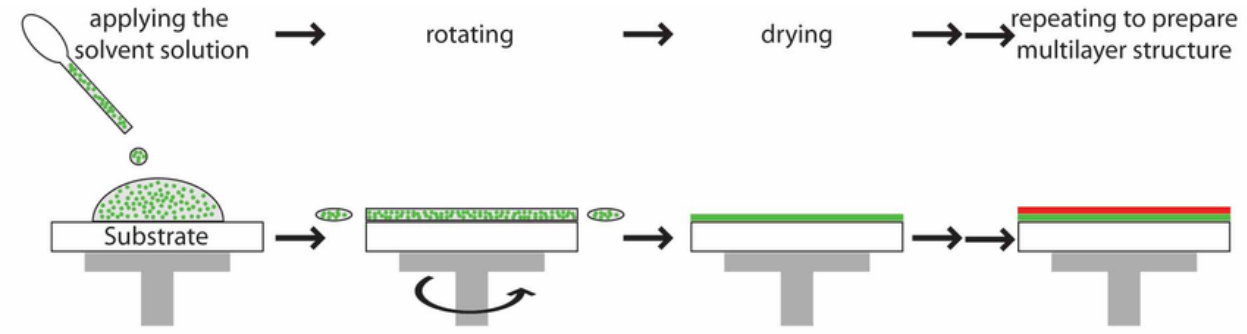

Figure 2.10 A schematic of spin-coat deposition.

As the deposited film is thinned by the centrifugal draining, it tends to be uniform since a balance occurs between the radially outward centrifugal force and the radially inward viscous force. Even with non-planar substrates, very homogeneous film thicknesses can be achieved.

Dip-Coating For this technique, the substrate to be coated is immersed in the solution and then withdrawn at a well-defined speed under controlled temperature and atmospheric conditions. A schematic is shown in Figure 2.11. In order to have a uniform film thickness, vibration-free mountings and smooth movement of the substrate are essential. Compared to spin-coating, dip-coating requires more sophisticated equipment.

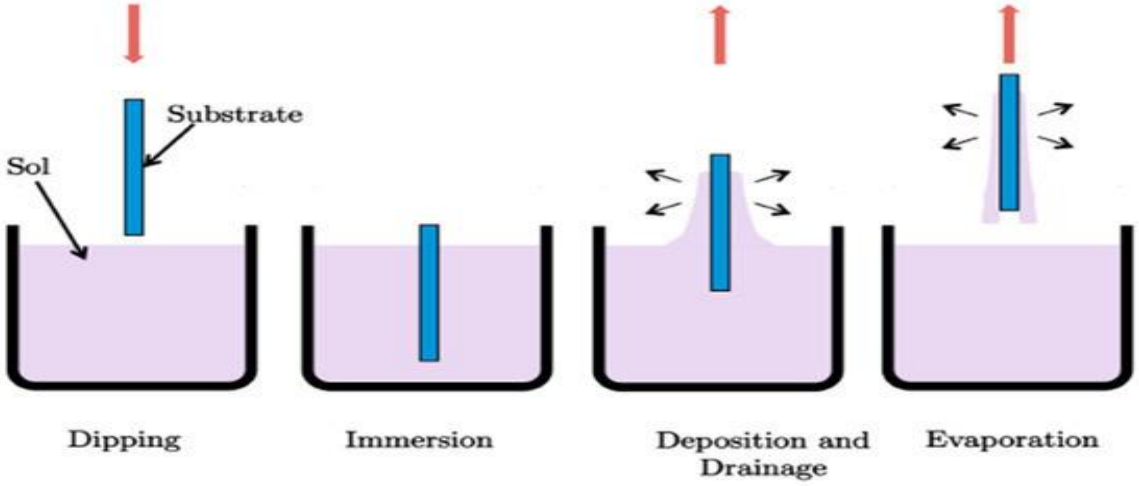

Figure 2.11 A schematic of dip-coat deposition.

2.6.2 Solgel spin coating technique for CCZO:

There are two types of spin coating methods:

Static process: At first solvent is applied and after that rotation started.

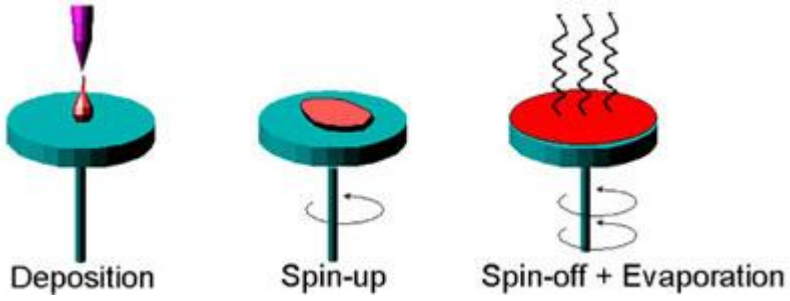

Figure 2.12: Static spin coating technique

Dynamic process: Rotation is started initially and at first the speed is low and after few seconds speed increases. Solvent is given during the low speed period.

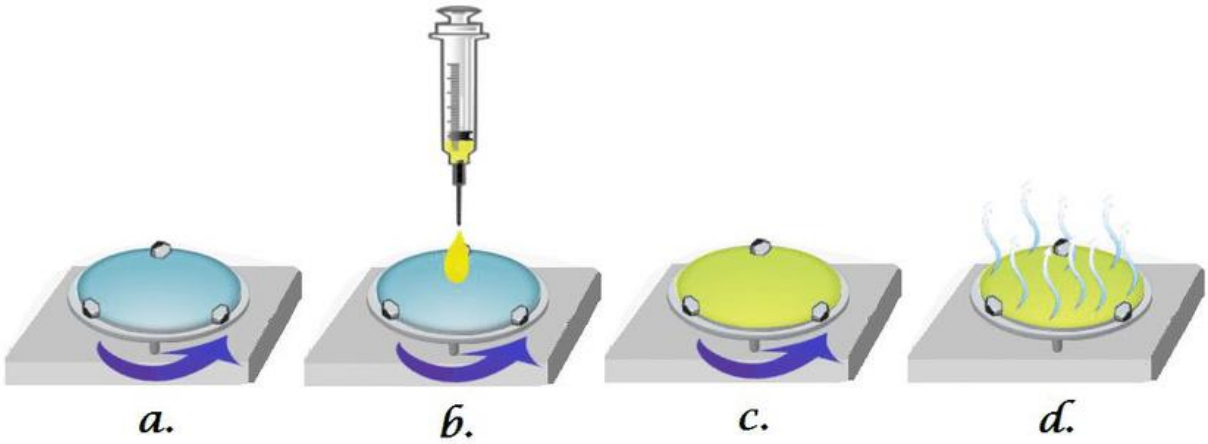

Figure 2.13: Dynamic spin coating technique

2.6.3 Advantages and Disadvantages of Spin Coating

The advantages of spin coating are the simplicity and relative ease with which a process can be set up, coupled with the thin and uniform coating that can be achieved. Due to the ability to have high spin speeds the high airflow leads to fast drying times, which in turn results in high consistency at both macroscopic and nano length scales.

The disadvantage of spin coating is that it is an inherently batch (single substrate) process and therefore has a relatively low throughput compared to roll-to-roll processes. The fast-drying times can also lead to lower performance for some particular nano-technologies which require time to self-assemble and/or crystallize. Finally, the actual material usage in a spin coating process is typically very low (at around 10% or less), with the rest being flung off the side and wasted. Whilst this is not usually an issue for research environments, it is clearly wasteful for manufacturing.

Despite these drawbacks, spin coating is usually the starting point and benchmark for most academic and industrial processes that require a thin and uniform coating.

2.6.4 Advantages and Disadvantages of the Sol-Gel Technique

Being a solution processable technique, sol-gel coatings offer many advantages for the fabrication of thin films over other techniques.

These include 1) Excellent control of the purity and stoichiometry of the coating solutions.

2) Ease of compositional modifications.

3) Suitability for deposition on large area substrates.

4) Simple and inexpensive equipment [42] [43].

Its disadvantage is that the sheet resistance of the films produced is usually at least one order of magnitude higher than that of the sputter-coated films [42]. One possible reason is that there are many more parameters which need to be optimized in sol-gel processes. Choice of precursors, number of layers deposited, drying temperature, annealing temperature and atmosphere could all play an important role in shaping the properties of the deposited thin films. Also, as sol-gel procedures are much more manual, good quality films are less reproducible than sputter-coated ones. However, by going through careful optimization and process control, this technique shows enormous potential in becoming the preferred low cost deposition method of the future [43].

2.7 High-entropy alloys (HEAs)

A pattern of alloy design emerged in near past decades as high-entropy alloys (HEAs) where five principal elements in equal or near equal atomic percent (at. %). The concept of high entropy introduces a new path of developing advanced materials with unique properties, which cannot be achieved by the conventional micro-alloying approach based on only one dominant element. Till date many HEAs such as CuNiCoFeMn, FeCoNiCrCu have been reported showing outstanding alloy properties [46].

2.7.1 Effects of High Entropy

From thermodynamics we know when different elements or compounds are mixed, in case of single phase homogeneous mixture, total free energy is changed by free energy of mixing

(ΔG_{mix}), which depends on the enthalpy of mixing [6] (ΔH_{mix}, could be exothermic or endothermic) and the entropy of mixing (ΔS_{mix}), that is:

$\Delta G_{mix}=\Delta H_{mix} - T\Delta S_{mix}$.

For regular solutions, $\Delta \boldsymbol{S}_{\text{mix}} = -\boldsymbol{R} \sum_{i=1}^{n} C_i \, lnC_i$ …….(2.3) Where R is the gas constant, C_i the molar fraction of the i_{th} element, and n the total number of the constituent elements Entropy is related to system disorder. Although total mixing entropy has four contributions such as configurational, vibrational, magnetic dipole, and electronic randomness, configurational entropy is dominant over other three excess contributions. Upon mixing, systems become more disordered, ΔS_{mix} always increases, causing ΔG_{mix} to become more negative. Alloys have traditionally been developed according to a 'base element' paradigm. This strategy begins with one and rarely two principal elements, such as iron in steels or nickel in superalloys, and a minor alloying approach is used to obtain alloys with enhanced properties. In sharp contrast, a novel paradigm for alloy design was proposed about a decade ago [48], which involves merely the mixing of multiple elements in an equimolar or near-equimolar composition to form alloys, thus eschewing the 'base element' concept. These designed multicomponent alloys were termed as 'high-entropy alloys' (HEAs) by Yeh et al. [4], which suggests the high configurational entropy of the random mixing of elements in these alloys. From equation x for five equiatomic mixture CoCuFeNiPd, CuNiFeCrMo: where entropy of mixing is $\Delta Smix=1.61R$.

So configurational entropy higher than 1.5R is large enough to compete with mixing enthalpy, and thereby these alloys are classified as high entropy stabilized single phase multicomponent alloys. Up until recently, this class of high entropy material was restricted to metals with relatively simple crystal structures within which all of the lattice sites are part of the entropic phase. In 2015, an entropy-stabilized oxide of the rocksalt crystal structure, $(Mg_{0.2}Zn_{0.2}Cu_{0.2}Co_{0.2}Ni_{0.2})O$, was fabricated by Rost et al. [6], extending HEAs from metals to ceramics with ionic bonds. More recently, high-entropy ultra-high temperature ceramics (HEUHTCs), e.g., $(Hf_{0.2}Zr_{0.2}Ta_{0.2}Nb_{0.2}Ti_{0.2})\ B_2$ and five other single-phase five-component metal diborides, and high-entropy functional ceramics, e.g., $Sr(Zr_{0.2}Sn_{0.2}Ti_{0.2}Hf_{0.2}Mn_{0.2})O_3$ and five other single-phase high-entropy perovskite oxides (HEPOs), have also been successfully synthesized [44,45] In all these cases, the configurational entropy was calculated using the following formula:

$$\boldsymbol{S}_{\text{config}} = -\boldsymbol{R}\,[(\sum_{i=1}^{n} C_i\, lnC_i\ )\ \boldsymbol{cation-site} + (\sum_{j=1}^{n} C_j\, lnC_j)\boldsymbol{anion-site}] \ldots\ldots\ldots$$

Where x_i and x_j represent the mole fractions of ions present in the cation- and anion-site, respectively. The contribution of the anion-site is expected to have a minor influence on S_{config}, given that only one anion is present.

However, it is interesting in the new class of high entropy stabilized $(Mg_{0.2}Zn_{0.2}Cu_{0.2}Co_{0.2}Ni_{0.2})O$ oxides that has a rocksalt structure with one of the face centered cubic (fcc) sublattices containing oxygen anions, and the other sublattice containing randomly arranged Mg, Co, Ni, Cu, and Zn cations in equi-atomic proportions. In addition to being an oxide, this system is a unique combination of an ordered and a disordered sublattice together within a single high entropy phase.

Now we will discuss about our ZnO where two interpenetrating cation and anion sublattices of the wurtzite structure exist together. Thinking beyond the literature, we have doped the cation sublattice with five various sizes of cations as stated earlier to deposit $(Cu_xCo_xMn_xMg_xNi_x)\ Zn_{1-x}O$ thin films by spray pyrolysis method. We targeted to generate randomly arranged Cu, Co, Mn, Mg, Ni cations in Zn sites to combine an ordered and a disordered sublattice together within a single high entropy phase where highest Sconfig. in case of 30% doping is 0.66R. Then evaluated the entropic contribution in ZnO single phase wurtzite structure. Also we investigated the sluggish diffusion effect and severe lattice distortion effect in single phase stabilization in deposited $(Cu_xCo_xMn_xMg_xNi_x)\ Zn_{1-x}O$ specially when doping concentration is high as 30% (where, 6% each dopant).

2.8 High-entropy oxides (HEOs)

Incorporating the concept from HEAs for the first time in 2015 Rost et al showed that a crystalline single phase rock salt structured oxide (XRD patterns shown in Figure 2.14) containing five transition metal ions in equiatomic amounts $(Mg_{0.2}Zn_{0.2}Cu_{0.2}Co_{0.2}Ni_{0.2}O)$ can be synthesized. This report widened the concept of high entropy stabilized structure not only bound in alloys; rather it can surround significantly the ceramic class type materials. Rost defined the new class of materials as high entropy stabilized oxides (HEOs) [6]. Subsequently in 2016 Djenadic et al synthesized few high-entropy rare earth oxides (REOs): (Ce,La,Pr,Sm,Y)O, (Ce,Gd,La,Pr,Sm,Y)O, (Gd,La,Nd,Pr,Sm,Y)O mixing the rare earth metal oxide nanopowders in

equimolar ratios [66]. More recently, high-entropy ultra-high temperature ceramics (HEUHTCs), e.g., $(Hf_{0.2}Zr_{0.2}Ta_{0.2}Nb_{0.2}Ti_{0.2})\ B_2$ and five other single-phase five-component metal diborides, and high-entropy functional ceramics, e.g., $Sr(Zr_{0.2}Sn_{0.2}Ti_{0.2}Hf_{0.2}Mn_{0.2})O_3$ and five other single-phase high-entropy perovskite oxides (HEPOs), have also been synthesized [49].

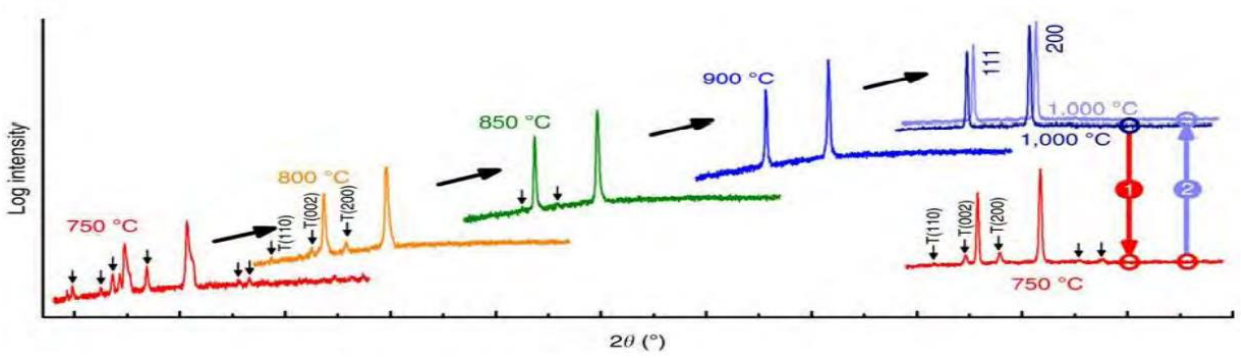

Figure 2.14: X-ray diffraction patterns for entropy-stabilized oxide consists of an equimolar mixture of MgO, NiO, ZnO, CuO and CoO. X-ray intensity is plotted on a logarthimic scale and arrows indicate peaks associated with non-rocksalt phases. Reproduced from ref. [6].

Till date high entropy stabilized ceramic materials other than oxides are also being explored to establish this concept of high entropy incorporation in the structure when multi-compounds are mixed in equimolar or near equimolar ratios and to reveal outstanding properties from this new class of material.

2.9 Characterization Principles

The deposited thin films have been characterized by their structural, stoichiometric, optical, electrical and magnetic properties. In this section, the characterization methods used in this work are reviewed briefly.

2.9.1 Structural studies

Here the techniques adopted to investigate the structural and morphological properties of thin films has been outlined. These techniques include X-ray diffraction (XRD) for structural

characterization and Scanning Electron Microscopy (SEM) for surface morphological characterization.

2.9.1.1 XRD

X-ray diffraction is the most precise technique for studying the crystal structure of solids, generally requiring no elaborate sample preparation and is essentially nondestructive [47]. Thin surface film, up to about 1000 Å thick, can be investigated using X-ray diffraction. Thicker films can be characterized by reflection high energy electron diffraction (RHEED). Diffracted patterns obtained from XRD can be compared with Joint Committee of Powder Diffraction Standards (JCPDS) that reveals the existence of different crystallographic phases in the film, their relative abundance, the lattice parameters and the preferred orientations. One has to determine whether a given deposit is a single crystal or polycrystalline either with a random distribution of orientation with respect to the coating plane. For a single crystal coating, it is important to know its orientation relationship with respect to the substrate X-ray diffraction is a suitable tool to determine the crystal structure of any unknown materials, whether the sample is a single crystal or polycrystals [47], either with a random distribution of orientations or with a preferred orientation with respect to the film plane.

When x-rays are scattered from a crystal lattice, peaks of scattered intensity are observed which correspond to the following conditions:

I. The angle of incidence = angle of scattering.
II. The path length difference is equal to an integer number of wavelengths.

Interference occurs among the waves scattered by the atoms when crystalline solids are exposed to X-rays. There are two types of interference depending on how the waves overlap one another. Constructive interference occurs when the waves are moving in phase with each other as shown schematically in Figure 2.15. Destructive interference occurs when the waves are out of phase. The relationship describing the angle at which a beam of X-rays of a particular wavelength diffracts from a crystalline surface was discovered by Sir William H. Bragg and Sir W. Lawrence Bragg and is known as Bragg's Law: $2d_{hkl} \sin\theta = n\lambda$ where, d_{hkl} is the distance between crystal plane determined for wurtzite structure ZnO unit cell by following relation:

$$\frac{1}{d_{hkl}^2} = \frac{4(h^2+hk+k^2)}{3a^2} + (\frac{l}{c})^2 \ldots\ldots\ldots\ldots\ldots(2.3)$$

a, c are lattice constants. θ is the X-ray incident angle; λ is the wavelength of the X-ray and n is a positive integer. Bragg's law also suggests that the diffraction is only possible when λ<2d.

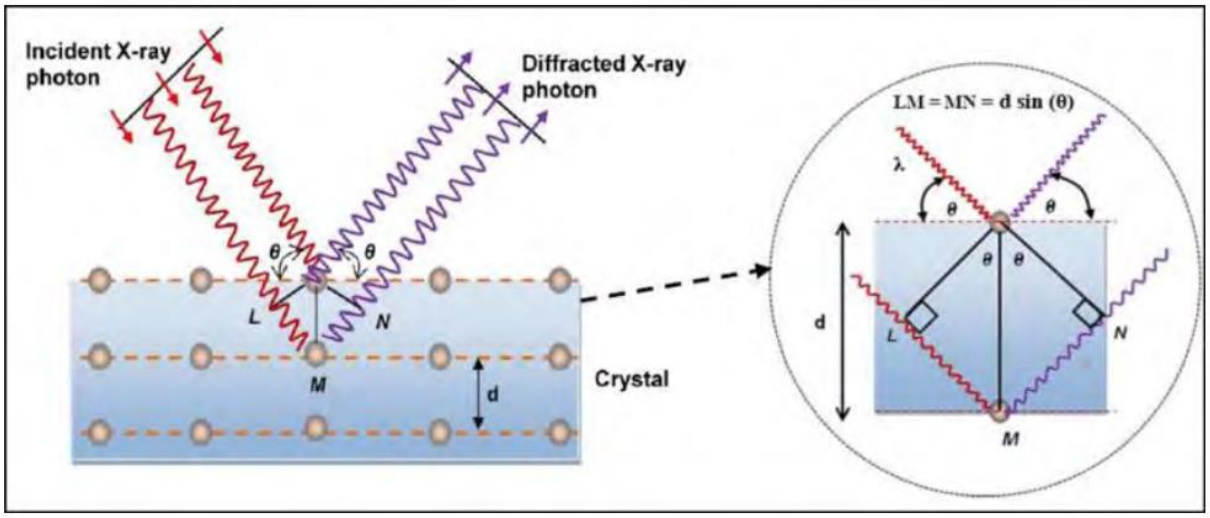

Figure 2.15: X-ray diffraction from Bragg planes. Reproduced from ref. [48]

From the width of the diffraction line, it is possible to estimate the crystallite size of the film [49]. The X-ay line broadening is commonly used to determine the crystallite size, which is known as Scherrer equation mentiomed as follows:

$D = k\lambda/\beta\cos\theta$

Where λ is the wavelength of the radiation used as the primary beam of CuKα (λ= 1.54178 Å), θ is the angle of incidence in degree and β is the full width at half maximum (FWHM) of the peak in radian. K is the the dimensionless constant with a typical value of about 0.9. The strain (ε) is determined by using following relations

$$\varepsilon = \frac{\beta cos\theta}{4} \ldots\ldots\ldots\ldots\ldots(2.4)$$

The dislocation density (δ) is defined as the length of dislocation lines per unit volume of the crystal, and it is estimated from the following relation using simple approach of Williamson and Smallman.

$$\delta = \frac{1}{D^2} \quad \ldots\ldots\ldots\ldots\ldots (2.5)$$

The structural characterization of the deposited films were carried out by X-ray diffractometer (Model: BRUKAR D8 ADVANCE) as shown on Figure 2.16.

Figure 2.16: Photograph of X-ray diffractometer (Model: BRUKAR D8 ADVANCE)

2.9.1.2 SEM

The scanning electron microscopy (SEM) is one of the most useful techniques for the investigation of surface morphology of thin film. High energy electron beam is used to excite the specimen that results in a number of interactions with the atoms of the target samples. The type of signals gathered in a SEM varies and can include secondary electrons, characteristic X-rays and back scattered electrons. The signals are collected and analyzed as shown in Figure so that an image can be constructed. The signals carry topological, chemical and crystallographic information of the samples surface.

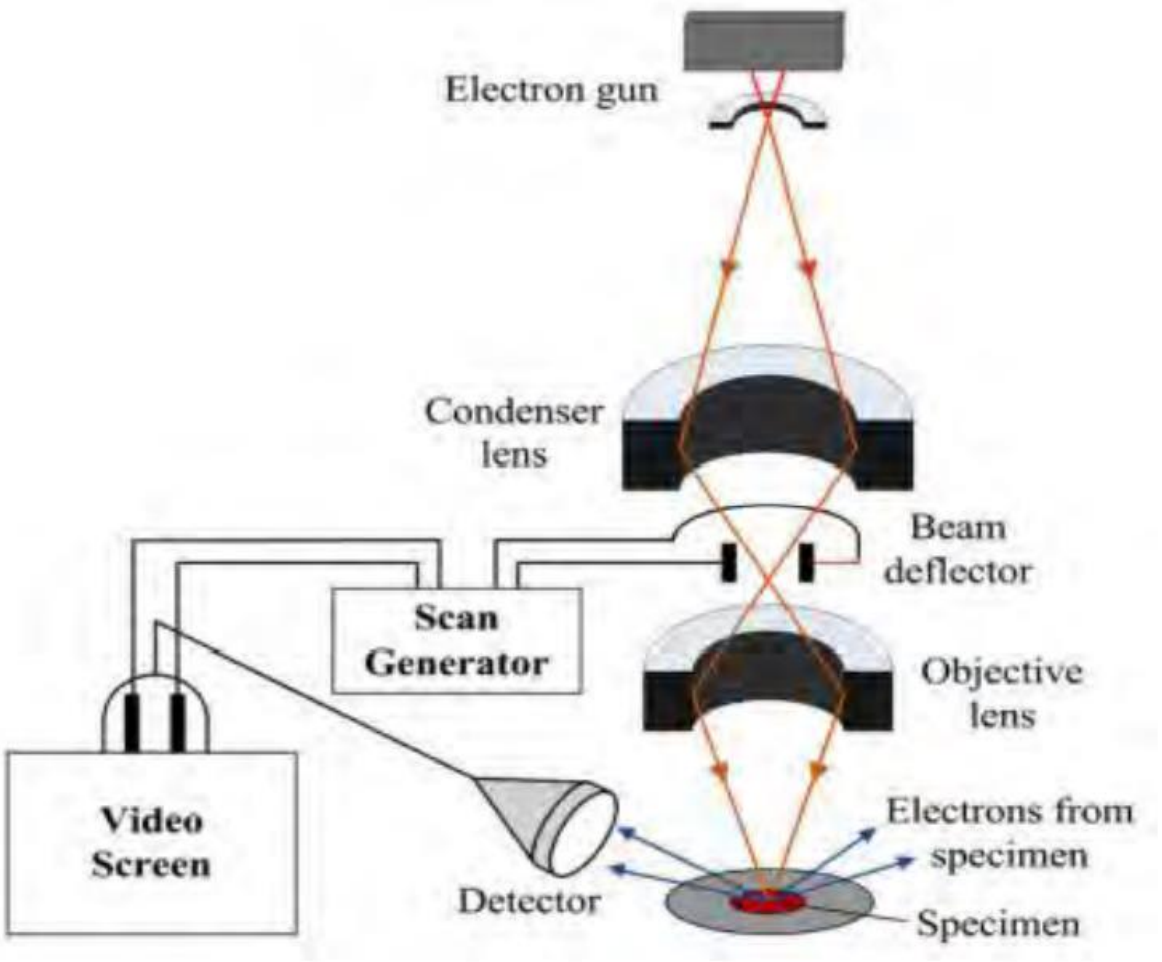

Figure 2.17: Schematic diagram of the SEM working principle. Reproduced from ref. [50].

In a SEM, these signals come not only from the primary beam impinging upon the sample, but from other interactions within the sample near the surface [50]. Figure 2.17 shows a schematic diagram of the SEM working principle. The SEM is capable of producing high resolution images of a sample surface in its primary use mode, secondary electron imaging. It also shows the capability of producing high resolution images of a sample surface in its primary use mode, secondary electron imaging. Due to the manner in which this image is created, SEM images have great depth of field yielding a characteristic three-dimensional appearance useful for understanding the surface structure of a sample. This great depth of field and the wide range of magnifications are the most familiar imaging mode for specimens in the SEM. Characteristic

Xrays are emitted when the primary beam causes the ejection of inner shell electrons from the sample and are used to tell the elemental composition of the sample. The back-scattered electrons emitted from the sample may be used alone to form an image or in conjunction with the characteristic X-rays as atomic number contrast clues to the elemental composition of the sample.

2.9.2 Optical studies

In this section the characterization techniques that were employed to investigate the optical properties of the thin films has been discussed.

2.9.2.1 UV-visible spectroscopy

In general, a study that involves the interaction of light and matter is defined as spectroscopy. It is the quantitative measurement of the reflection or transmission properties of a material as a function of wavelength [51]. UV-Visible (UV-Vis) spectroscopy is a type of absorption spectroscopy in which light of ultra-violet region (200-400 nm) is absorbed by the molecule which results in the excitation of the electrons from the ground state to a higher energy state. The energy of the ultraviolet radiation that is absorbed is equal to the energy difference between the ground state and higher energy states. UV-Vis spectrophotometer measures the intensity of light passing through a sample (I), and compares it to the intensity of light before it passes through the sample (I0). A schematic operating mechanism diagram of UV-Vis spectrophotometer has been shown in Figure 2.18. The ratio (I/I0) is called the transmittance, and is usually expressed as a percentage (%T) [52]. The absorbance A is based on the transmittance. The UV-visible spectrophotometer can also be configured to measure reflectance. In this case, the spectrophotometer measures the intensity of light reflected from a sample (I), and compares it to the intensity of light reflected from a reference material (I0). The ratio (I/I0) is called the reflectance, and is usually expressed as a percentage (%R). The measurement of the transmission or reflection of a sample provides a satisfactory way to determine the form of the absorption edge. The absorption edge and energy band gap (E_g) can be determined from the transmission measurement. When a radiation is incident on a thin film material with energy equal or greater than that of the band gap, absorption of the photons can take place and electrons can be raised in

energy from the valence band to the conduction band, creating electron-hole pairs. The material can transmit the photons having energy less than the band gap of the semiconductor, as the energy is insufficient to create an electron hole pair.

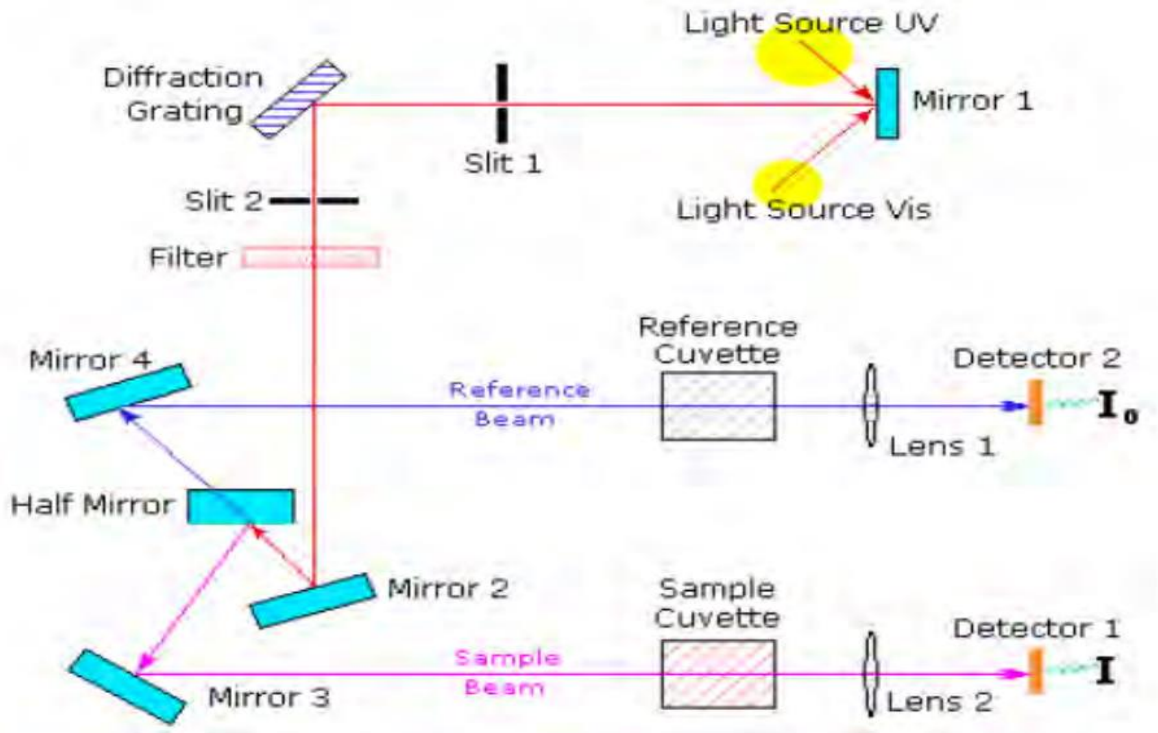

Figure 2.18: A scheme of UV-Vis spectrophotometer operating mechanism. Reproduced from ref. [52].

The ability of a material to absorb photons of a given wavelength is measured quantitatively by the optical absorption coefficient (α), measured as: α = 2.303A/d, where d is film thickness and A is absorbance.

The optical absorption coefficient and energy band gap (Eg) relation is known as Tauc's relation [70]; can be written for direct band gap material as:

$$\alpha h\upsilon = (h\upsilon - E_g)^{1/2} \ldots\ldots\ldots\ldots\ldots (2.6)$$

Other parameters such as film thickness (d), optical conductivity etc. also can be measured from the parameters and results found above. Film thickness can be measured from optical reflectance data by Swanepoels method using the following relation:

$$d = \frac{\lambda_1 \lambda_2}{2(n_1\lambda_2 + n_2\lambda_1)} \ldots\ldots\ldots\ldots\ldots (2.7)$$

Where n_1 and n_2 are the refractive indices at two adjacent reflectance maxima (or minima) at the wavelength λ_1 and λ_2, respectively.

2.9.2.2 FTIR

Infrared spectroscopy (IR) is one of the most powerful analytical tools to identify the presence of certain functional groups in a molecule and to detect the presence of specific impurities present in inorganic and organic compounds. From the IR analysis, it is possible to identify the functional groups on surfaces and adsorbents and molecular composition of the materials. An infrared spectrum represents a fingerprint of a sample with absorption peaks which correspond to the frequencies of vibrations of the bonds of the atoms making up the material. Infrared spectroscopy is based on absorption of IR radiation causing transition in the sample from one vibrational state to another higher energy vibrational state. Consequently, the infrared spectrum is a set of absorption bands whose intensity and frequency provide information of structure and bonding in the molecule.

FTIR instruments employ interferometer techniques in the collection of spectral information and the spectrum is obtained as an inverse Fourier-Transform of the interferogram [53]. More comprehensively to say that: a radiation emitted from the light source is splitted into two portions with a beam splitter in the interferometer. The fixed and moving mirrors reflect each of the beams back to the beam splitter, where the two beams recombine into one and fall on the detector. The two beams combine constructively or destructively, varying as the optical path difference, when the moving mirror is moved. When the combined beam is transmitted through the sample, it is detected as an interferogram and contains all infrared information on the sample.

The infrared spectrum is obtained from the interferogram by the mathematical process of Fourier transformation. This operating principle has been shown schematically in following the Figure.

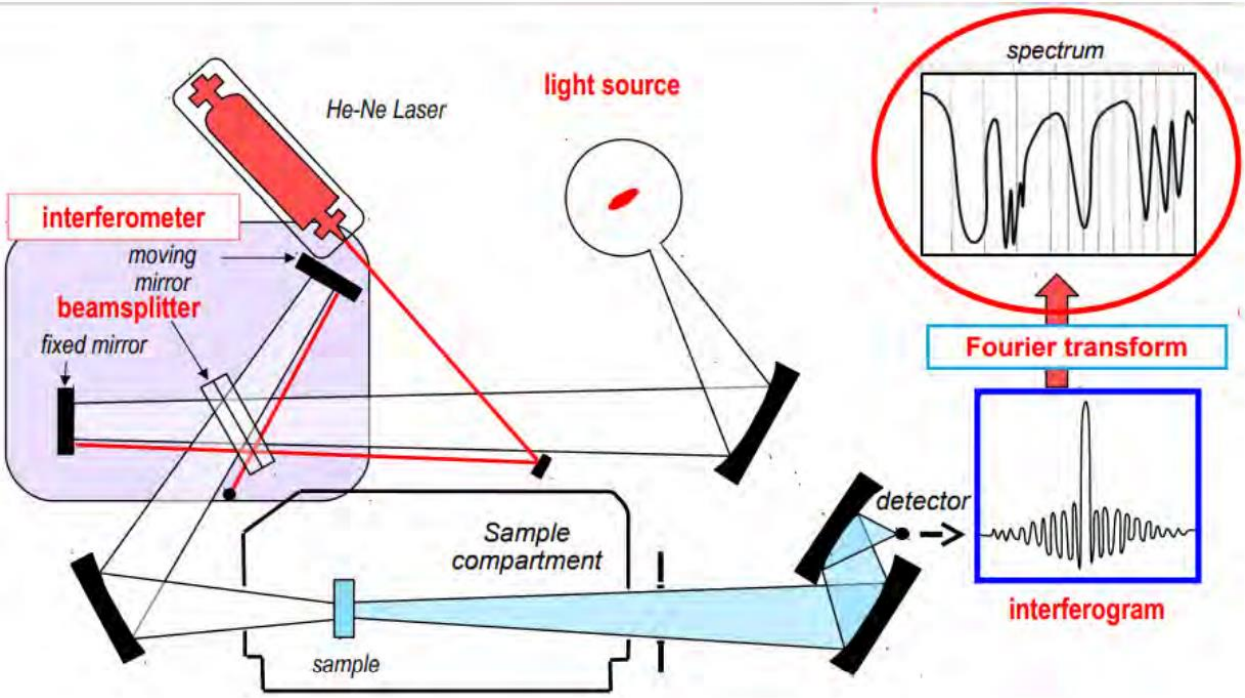

Figure 2.19: A schematic of FTIR spectroscopy. Reproduced from ref. [53].

Chapter III

Experimental Details

3. Introduction

ZnO thin films have been deposited by spin coating fabrication technique. Spin coating has the ability to create very fine, thin, and uniform coatings; however, it has the drawback of making large area samples difficult. The desired film thickness can be obtained using the spin-coating technique. Spin coating technique is very simple and cost effective. The spin coater we used in our laboratory is shown in following figure 3.10. Number of rotation and time for the rotation is set up before dropping the solution. The volume of solution, drop technique etc. are controlled manually. Zinc acetate, 2methoxyethanol, monoethanolamine were used to deposit pure ZnO thin film. In addition zinc acetate, 2methoxyethanol, monoethanolamine and other five dopant salts mixed solutions were used to have the rest CCZ10, CCZ20 and CCZ30 thin films.

3.2 Film synthesis

3.2.1 Raw materials and their contribution

- Starting Material
  - Zinc acetate dehydrate (ZAD)[$Zn\ (CH_3COOH)_2.2H_2O$]
  - Molecular weight 219.49 gm/mol

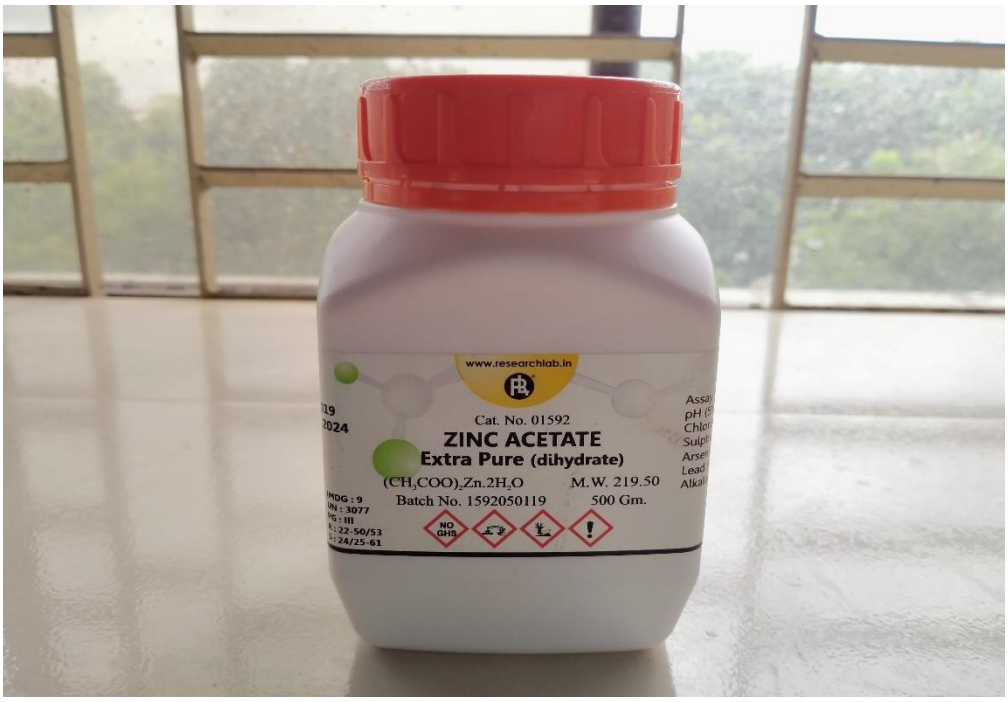

Figure 3.1: Starting Material (Zinc Acetate Dehydrate)

- Solvent
    - 2-methoxy ethanol (MOE) ($CH_3OCH_2CH_2$OH)
- Stabilizer
    - Mono-ethanol-amine (MEA) [$(HOCH_2CH_2)NH_2$]
    - Molecular weight 61.08 gm/mol
    - Density 1.015 gm/cc

Figure 3.2: Solvent and Stabilizer (2-methoxy ethanol & Mono-ethanol-amine)

- Doping Material
    - Hydrated Cobalt nitrate [Co$(NO_3)_2$ .6H_2O]
    - Nickel Nitrate [Ni$(NO_3)_2$. 6H_2O]
    - Manganese Sulphate [MnSO_4. H_2O]
    - Magnesium Nitrate [Mg$(NO_3)_2$. 6H_2O]
    - Copper Nitrate [Cu$(NO_3)_2$. 3 H_2O]

Figure 3.3: Doping Materials

3.2.2. Other ingredients

- Glass (75mm*25mm*1mm)
- Washing agent:
    - Acetone
    - Ethanol
    - De-ionized water
- Beaker (200 ml-2 ,500 ml -1)
- Magnetic stirrer
- Hot plate
- Ultrasonic Cleaner
- Thermometer
- Others

(a)

(b)

(c)

(d)

Figure 3.4: (a) Ultrasonic Cleaner (b) Hot Plate (c) Micro-pipet and (d) Glass Cutter

3.2.3. Requirements of Raw Material

Table 3.1:

Composition	Raw Materials	Amount (gm)	Total(gm)
Pure ZnO film	$(CH_3COO)_2Zn.2H_2O$	1.75592	1.75592
CCZO10	$(CH_3COO)_2Zn.2H_2O$	1.75592	1.95792
	$Cu(NO_3)_2.3H_2O$	0.0390	
	$Co(NO_3)_2.6H_2O$	0.0470	
	$Ni(NO_3)_2.6H_2O$	0.0475	
	$Mg(NO_3)_2.6H_2O$	0.0410	
	$MnSO_4.H_2O$	0.0275	
CCZO20	$(CH_3COO)_2Zn.2H_2O$	1.75592	2.16
	$Cu(NO_3)_2.3H_2O$	0.0780	
	$Co(NO_3)_2.6H_2O$	0.0940	
	$Ni(NO_3)_2.6H_2O$	0.0949	
	$Mg(NO_3)_2.6H_2O$	0.0820	
	$MnSO_4.H_2O$	0.0552	
CCZO30	$(CH_3COO)_2Zn.2H_2O$	1.75592	2.36232
	$Cu(NO_3)_2.3H_2O$	0.1171	
	$Co(NO_3)_2.6H_2O$	0.1411	
	$Ni(NO_3)_2.6H_2O$	0.1424	
	$Mg(NO_3)_2.6H_2O$	0.1231	
	$MnSO_4.H_2O$	0.0827	

ZAD=0.4M

ZAD and MEA molar ratio= 1:1

3.2.4. Solution Preparation

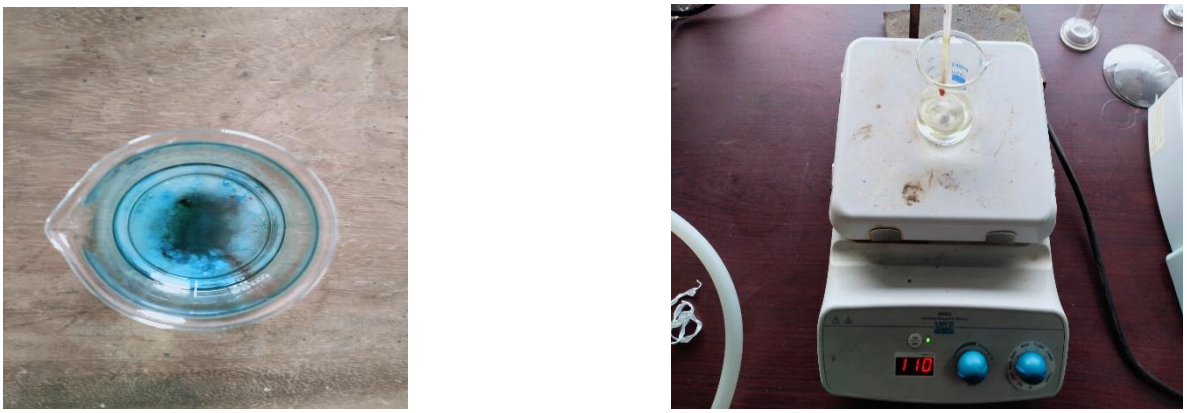

(a) (b)

Figure 3.5: (a) Initial Solution and (b) Solution stirring for 1 hour

Steps in detail:

Weighting:

- Weighting should be as perfect as possible
- Before weighting, spoons should be washed with de-ionized and acetone
- The powders should be weighted just before experiment, otherwise contamination can be occurred.

Figure 3.6: Weighting Procedure

Mixing:

- At first solvent is added in a washed beaker (Beaker is also washed with de-ionized and acetone)
- Then starting material and doping material are added.
- Finally, stabilizer is added.

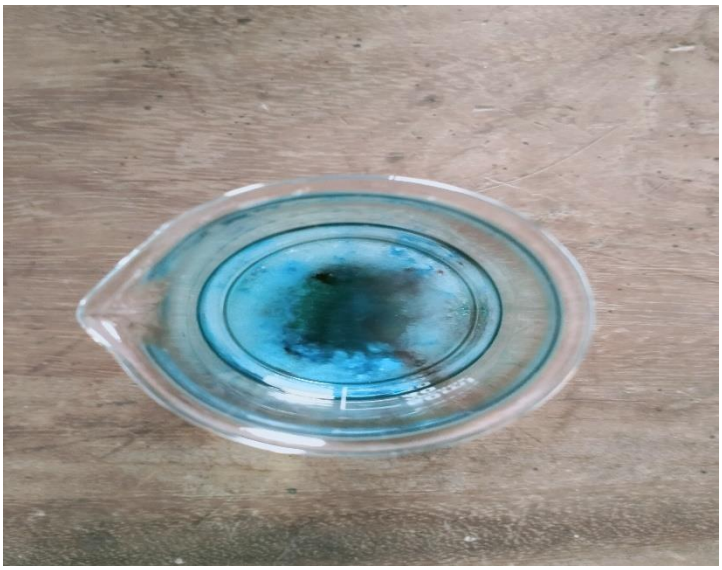

Figure 3.7: Solution After Mixing

Stirring:

- Stirring is done at 400 rpm at 80° C.
- As our solution quantity is small, we used a small sized magnetic stirrer.
- Temperature control is very important. Thermometer is used for this. When hot plate indicated 115° C, thermometer indicates 80° C.
- After when thermometer indicates 80° C, time counting is started.
- After 1 hour stirring, the solution is covered with aluminium foil and kept for aging for 24 hours.

Figure 3.8: Solution stirring for 1 hour

Possible chemical reactions that take place-

$(CH_3COO)_2\ Zn.2H_2O + H_2O \xrightarrow{\text{Decomposed at 200°C}} ZnO + CO_2\ (g) + CH_4\ (g) + \text{steam (g)}$

For CCZO10, CCZO20 and CCZO30 possible chemical reactions can be noted as:

$(CH_3COO)_2\ Zn.2H_2O + Cu(NO_3)_2.3H_2O + Co(NO_3)_2.6H_2O + Ni(NO_3)_2.6H_2O + Mg(NO_3)_2.6H_2O + MnSO_4.H_2O$

$\xrightarrow{\text{Decomposed at 200°C}} (Cu_xCo_xNi_xMg_xMn_x)Zn_{1-5x}O + CO_2\ (g) + NO_2\ (g) + CH_4\ (g) + \text{steam (g)}$

3.2.5. Glass Preparation

- Glass is prepared by cleaning with acetone, ethanol, de-ionized water by cotton. Ultra-sonification with de-ionized water, ethanol, acetone.
- At first silica glass is cut in appropriate size by glass cutter.
- Then the glass is brushed with detergents and washed with water.
- Then the glass is ultrasonified with de-ionized water for 5 min.
- After that the glass is ultrasonified with ethanol, acetone and again de-ionized water, each one is for 5 min
- After each drying stage the glass substrate is dried using hotplate.
- Now the glass substrate is ready for coating.
- 60% efficiency of producing uniform film depends on glass cleaning properly.

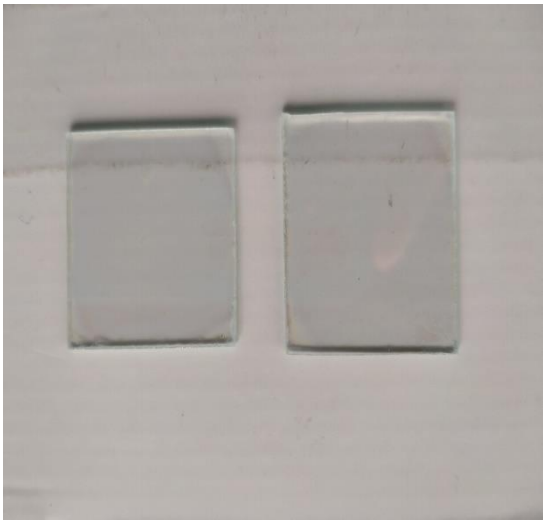

(a) (b)

(c)

Figure 3.9: (a) Glass Slide; (b) Glass Slide After Cutting and (c) Dipped in distilled water, ethanol and acetone

3.2.6. Spin coating

- At first static coating technique is applied. But unfortunately, film quality was not good. Film was not uniform. Then dynamic spin coating technique is applied. Speed is modified experimentally.
- Solution is given using 1ml pipette. Spin coater speed is modified at1000 rpm for 10 second, then 3000 rpm for 20 sec. At first speed is low because the solution is given. To reduce scattering of the solution. Spin coater should be covered with aluminium foil.

- Glass substrate is kept at the right place. Vacuum on is done by switching.

Figure 3.10: Spin Coater

- Then on button is pressed and 0.05 ml solution is given on the substrate.
- After 30 seconds rotating would be stopped. Then we have to off vacuum.
- After drying, second layer is given.

3.2.7. Drying

After spin coating, drying for 5 min at 200 ℃.At first this step was done using furnace. But there is a great chance of contamination with the furnace atmosphere. And it was really uncomfortable. Then we started drying in the hot plate.

- At first hot plate temperature is fixed at 200℃.
- After each coating step the glass substrate is taken to hot plate.
- 5 min is the drying period.
- After drying, the sample is cooled and readied for the 2nd layer.

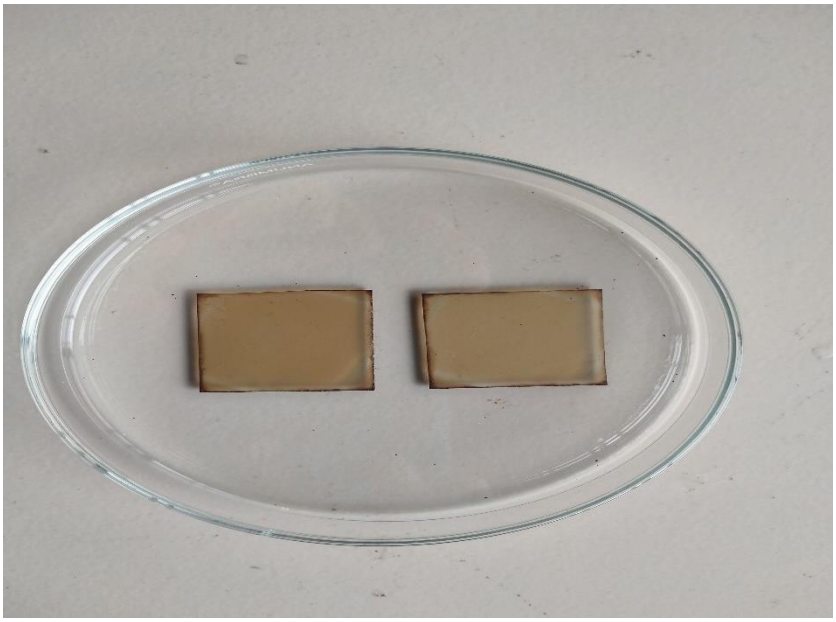

Figure 3.11: Sample after Drying

3.2.8. Annealing

- For annealing the thin film Protherm furnace was used. It took very little time about 20 minutes to reach 500° C. Then 2 hour holding period and after that furnace cooling
- Masking tape is used for making a step for measuring thickness with profilometer. But the masking tape was vaporized during high temperature annealing. Thus, film contamination occurred. For recovering that problem, we used at first better quality masking tape. After drying stage, the masking tape was removed as it cannot withstand the high temperature of annealing.

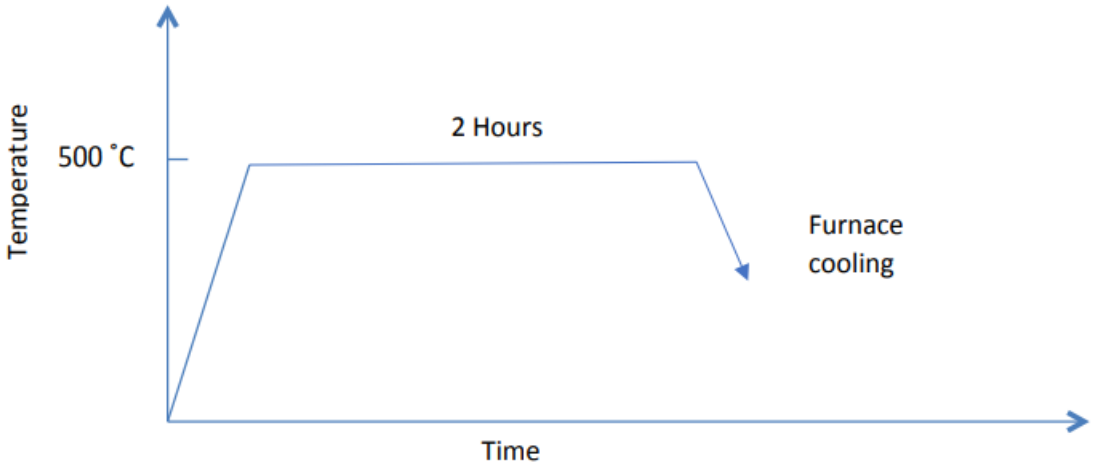

Figure 3.12: Annealing graph

Chapter IV

Result & Discussion

4. Introduction

The various characterization data have been used to assess the qualities and prospective uses of the deposited films. The findings and discussion of the numerous experimental research, including structural, morphological, optical and electrical properties of $(Cu_xCo_xNi_xMg_xMn_x)Zn_{1-5x}O$ thin films have been demonstrated step by step.

4.1 Structural properties

The X-ray diffraction patterns of pure ZnO thin film is shown in figure 4.1. From this figure well crystallized diffraction peaks were observed. The peak pattern indicates the crystal structure was hexagonal wurtzite structure according to Joint Committee of Powder Diffraction Standards data (JCPDS card number 96-101-1260).

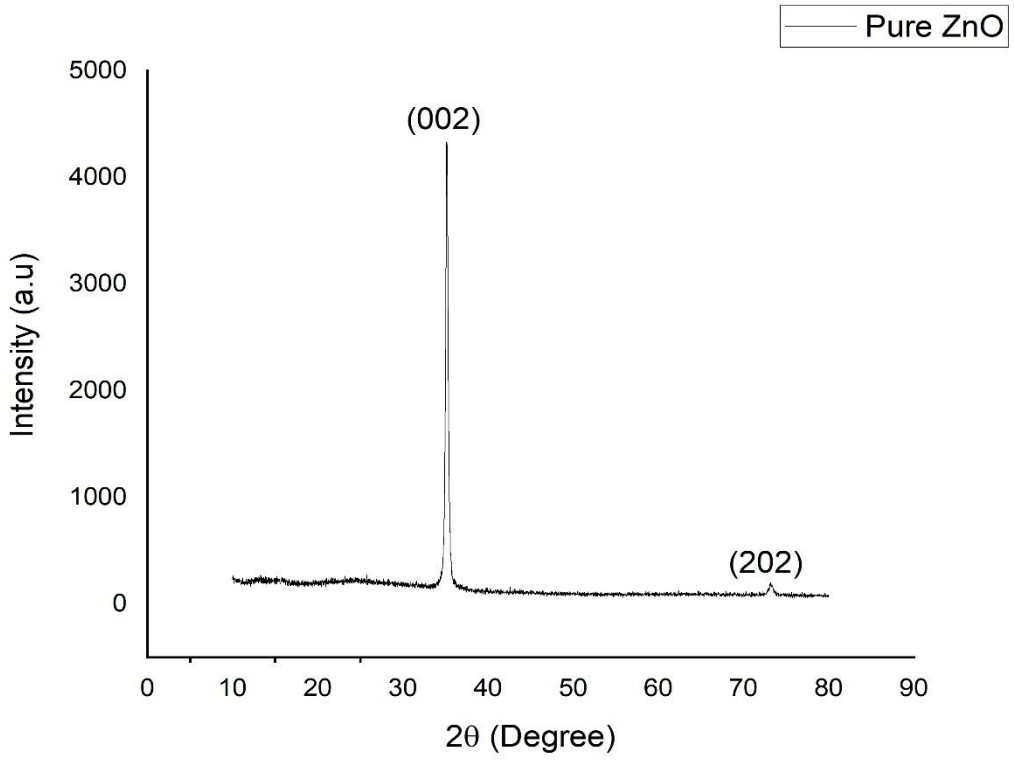

Figure 4. 1: (a) XRD graph of pure ZnO thin film sample

We can see from the figure that the peak postion is well matched with ZnO hexagonal wurtzite structure peak position. There is no other impurities, the XRD peak only shows the ZnO structure peak.[54]

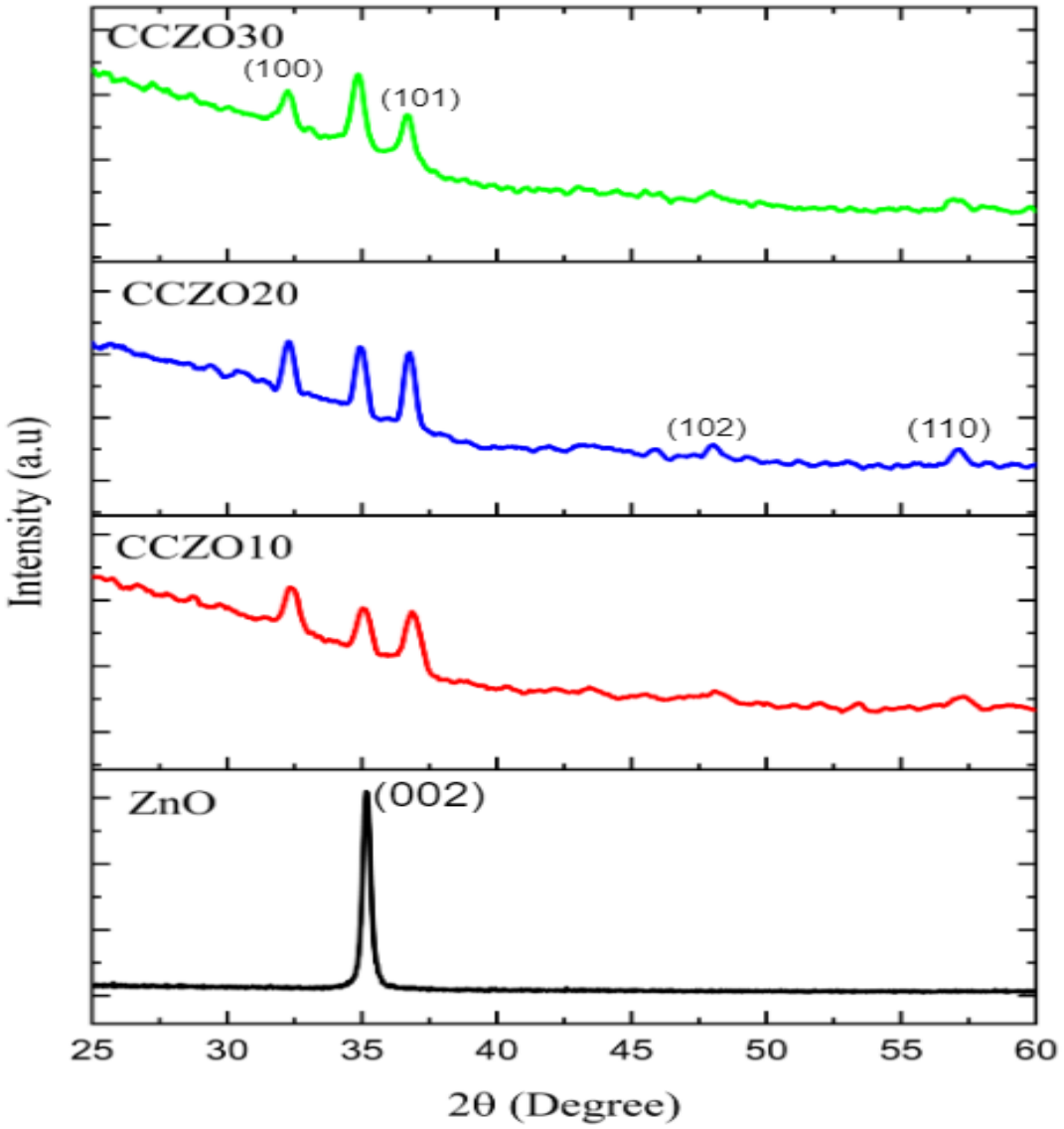

Figure 4. 1: (b) XRD graphs of all pure ZnO, CCZ10, CCZ20, CCZ30 thin film samples

From figure 4.1 (b) we can see adding five elements as dopant in ZnO lowers the intensity of the peak compared to pure ZnO. . This indicates that the crystallinity of ZnO is decreased by adding doping elements. But the (002) plane peak intensity is increasing by increasing the doping concentration.

Table 4. 1: XRD data for all the tested samples indexed with JCPDS card number 96-101-1260 for wurtzite ZnO.

ZnO Wurtzite Structure		Pure ZnO		CCZO10		CCZO20		CCZO30	
2θ	hkl	2θ	Relative Intensity	2θ	Relative Intensity	2θ	Relative Intensity	2θ	Relative Intensity
34.228	(002)	34.291	136.4	35.009	41.5	35.144	43.2	34.820	44.5
31.749	(100)			32.225	43.4	32.329	44	32.081	39.5
36.257	(101)			36.801	42.5	36.925	44.5	36.627	30.8
47.257	(102)			48.316	12.7	48.493	12.3	48.068	12.5
	(110)			57.460	10.5	57.657	13.4	57.187	12.6
	(103)			63.970	10.1	64.224	10.2	63.612	10.6

The interplanar spacing d_{hkl} increases with dopants addition in the ZnO structure as it proved from Bragg's law of diffraction: $2d_{hkl} \sin\theta = n\lambda$ which implies that the decrement of 2Ɵ value increase interplanar spacing d. The d_{hkl} for wurtzite structure ZnO unit cell is calculated from the equation (4.1) given below:

$$\frac{1}{d_{hkl}^2} = \frac{4(h^2+hk+k^2)}{3a^2} + \left(\frac{l}{c}\right)^2 \ldots\ldots\ldots\ldots\ldots (4.1)$$

In all of the samples, there was only one additional peak that was ZnO wrtzite structured, indicating that there was only one phase of wurzite ZnO. Complete doping is ensured by a slight dispositioning of doped samples peaks when compared to pure ZnO. Additionally, doping was caused by the substitutional replacement of the Zn cation (r_{zn2+}=0.074 nm) by the cations of Cu, Co, Mn, Mg, and Ni (r_{Cu2+}=0.073 nm, r_{Co2+}=0.072 nm, r_{mn2+}=0.082 nm, r_{Mg2+}=0.066 nm, and r_{Ni2+}=0.078 nm). As smaller sizes Cu, Mg replace Zn that may result in unit cell volume decreament.

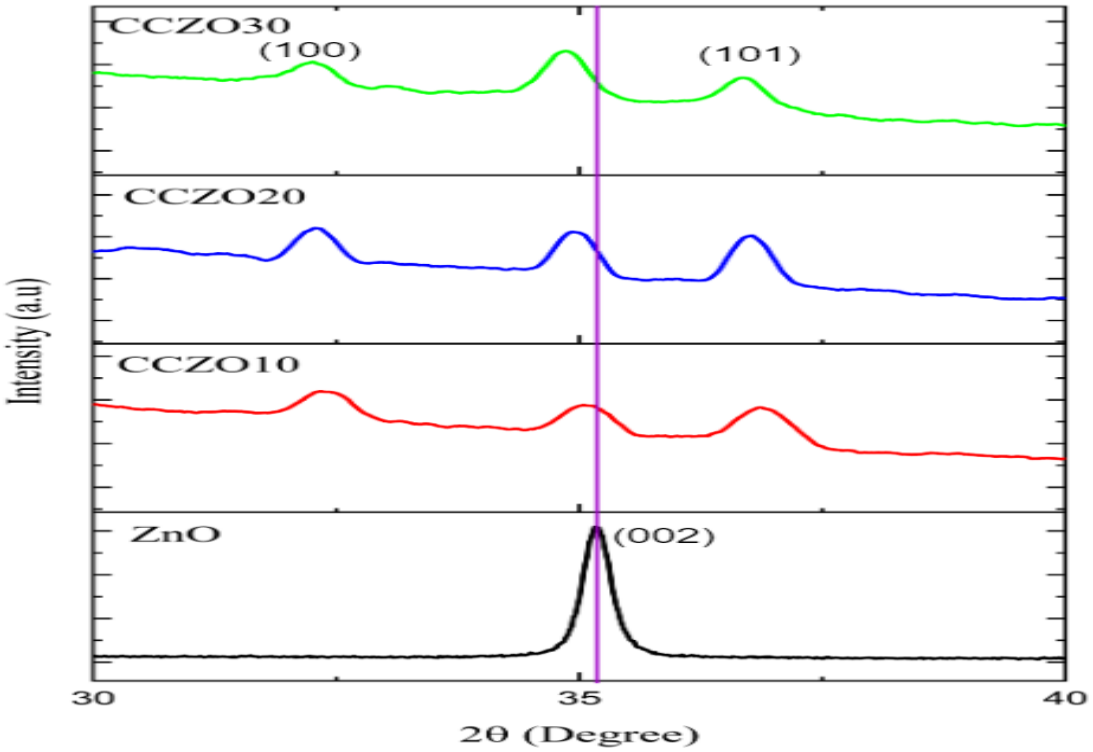

Figure 4. 1: (c) Peaks shifting towards lower diffraction angle with doping

After doping with five elements in ZnO , shifting of the peak position towards lower 2θ value is observed.

Since the preferential crystallographic growth of spray deposited thin film crystal along (002) plane, found from the Table of 4.1 and Figure 4.1 (b), full width at half maximum intensity (FWHM), β of the (002) diffraction peak was utilized in Scherrer equation $D = k\lambda/ \beta\cos\theta$, to calculate the average crystallite size, D of pure ZnO, CCZO10, CCZO20, CCZO30 thin films, where k is the dimensionless constant with a typical value of ~0.9, λ is the wavelength of Cu Kα radiation with the value of 1.5418 Å and θ is the Bragg angle of (002) diffraction peak. Since with the doping elements addition characteristics XRD peaks broadens shown in Figure 4.1 (b); crystallite size (D) would be decreased [55]. The crystallite size values have been measured as: 23.6, 20.72, 24.78 and 25.05 nm respectively. This can be attributed to the increase of produced nucleation centers due to higher concentration and multi elements doping [56]. When the D

values has been determined, the strain (ε) and dislocation density (δ) are determined by using following relations.

$$\varepsilon = \frac{\beta cos\theta}{4} \ldots\ldots\ldots\ldots$$

$$\delta = \frac{1}{D^2} \ldots\ldots\ldots\ldots\ldots$$

Among all the samples crystalline properties of CCZO10,CCZO20 and CCZO30 samples downfall as diffraction intensities of all peaks degenarate than pure ZnO samples and preferred growth orientation does not change from (002). As with higher doping of 20 and 30% in rest two samples peaks intensity increases with low background noise which indicates increasing crystallinity and reducing stress.

Table 4. 2: Refined structural parameters, calculated crystallite sizes (D), interplaner spacing, strain, dislocation density and Reitvelt fitting parameters.

Parameters	Sample			
	Pure ZnO	CCZO10	CCZO20	CCZO30
D (nm)	23.6	20.72	24.78	25.05
a (Å)	3.3510	3.2050	3.1950	3.2190
c (Å)	5.2260	5.1220	5.1030	5.1490
c/a	1.56	1.6	1.597	1.6
d_{002} (Å)	2.61300	2.56100	2.55150	2.57450
V ($Å^3$)	50.82	45.56	45.11	46.21
Density (g/cm^3)	5.32	5.93	5.99	5.85
Dislocation density * 10^5 lines/m^2	1.795	2.33	1.63	1.594
Strain (ε) *10^{-3}	3.65	4.84	4.52	4.45

4.2 Morphological properties

Surface morphological studies of the undoped ZnO and doped CCZO10, CCZO20 and CCZO30 films have been carried out from scanning electron micrographs (SEM). Figures 4.2 (a-d) shows the SEM images of all the undoped and doped ZnO thin films. The micrographs indicate that, during deposition of ZnO and doped ZnO by spraying the solution onto heated substrates, the growth has taken place by nucleation and coalescence process. Both spherical and rod like textures of grains were observed in pure ZnO film surface morphology. This

nano rod texture may be due to particle agglomeration effect. But in all the doped samples this morphology changed to flakes like appearance. Such type of morphology well match with the report of Deshpande's work of ZnO spray deposited thin film [57]. Flake shaped particle size reduced with doping concentration enhancement as observed from above SEM images. This size reduction may be the effect of crystallite side decrement as calculated in XRD results.

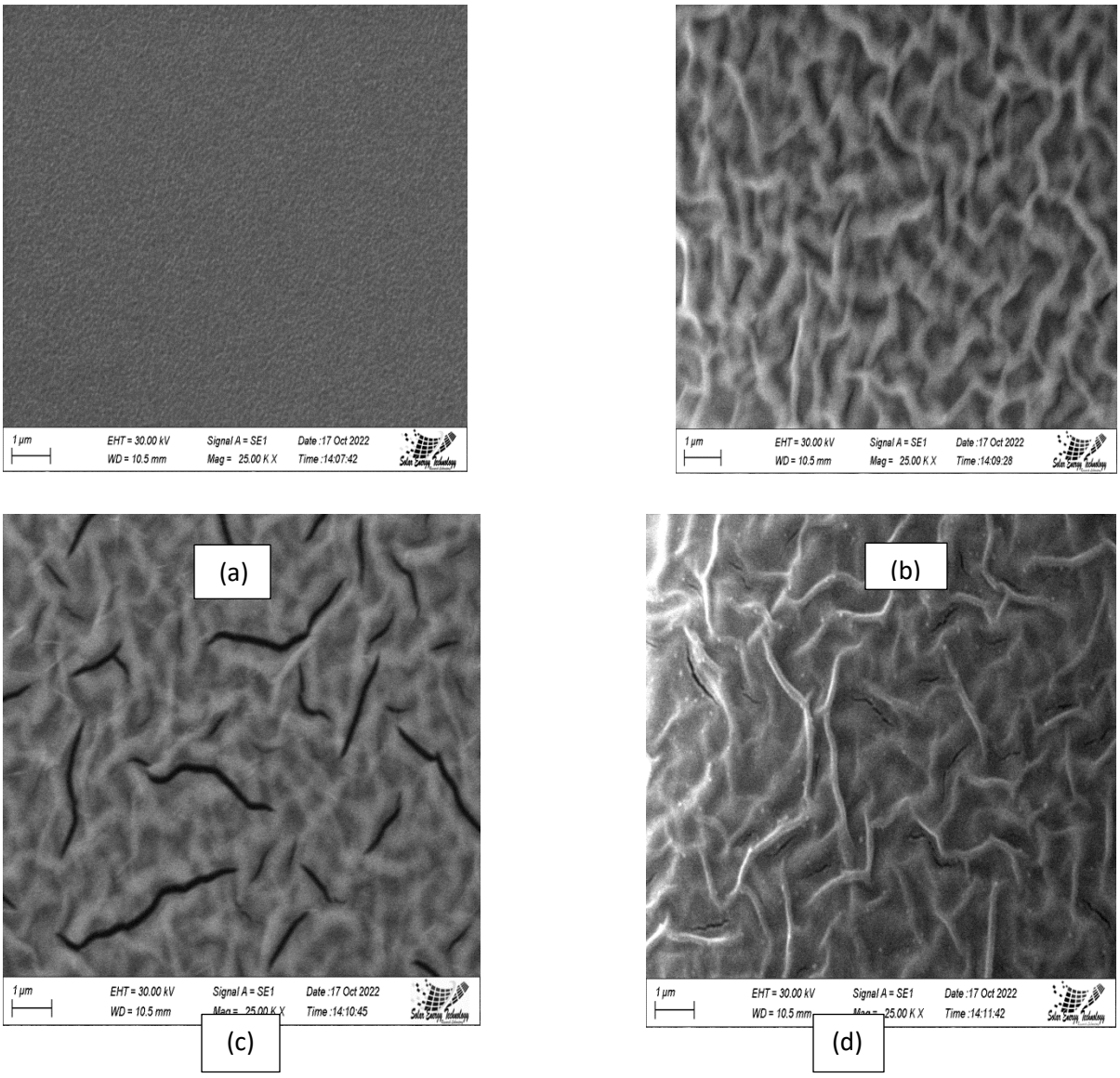

Figure 4.2: Scanning Electron micrographs (SEM) of (a) Pure ZnO (25,000X), (b) CCZO10 (25,000X), (c) CCZO20 (25,000X) and (d) CCZO30 (25,000X)

The dopants (Cu, Co, Mn, Mg and Ni) atoms may have raised nucleation sites; thus hindered the growth process resulting into the formation of smaller grains.

4.3 Optical properties

4.3.1 UV-vis results

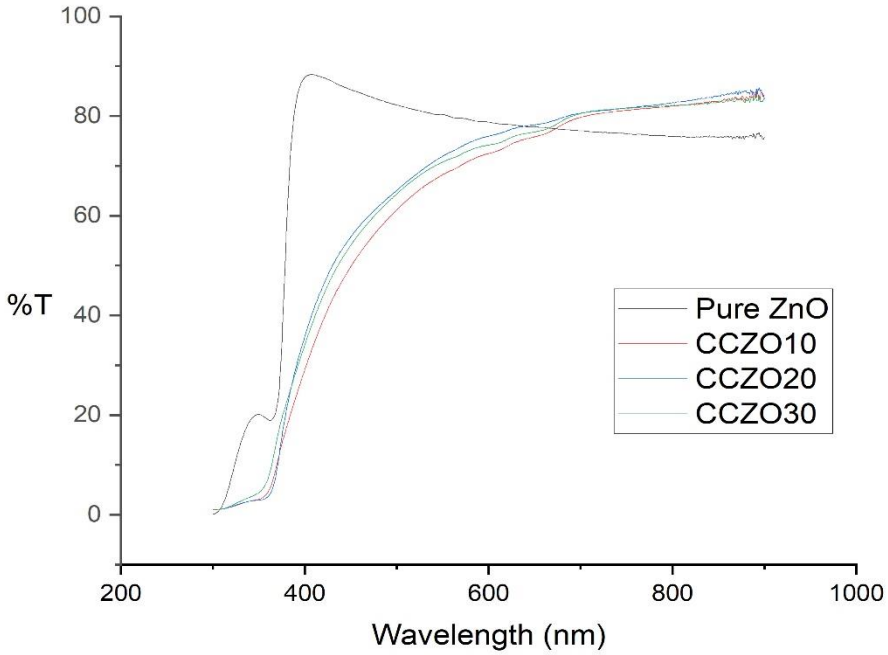

Figure 4.3: (a) UV-vis transmission spectrum of Pure ZnO, CCZO10, CCZO20 and CCZO30 films

Optical transmission spectra of the pure and doped ZnO films recorded in the wavelength region of 300–900 nm is shown in Figure 4.3. The transmission is found to be maximum for CCZO30 film sample about 82% and then though decreased for CCZO20 and CCZO10 film; the transmittance value is less than 80% in pure ZnO. This indicates that CCZO10, CCZO20, CCZO30 films are highly transparent and can be used for window layers in solar cells [58]. Less light scattering was the cause of the CCZO10, CCZO20 and CCZO30 materials increased

transmittance. A sharp transmittance edge has been observed for pure ZnO film around 380 nm and then suddenly the transmittance decreased under 80% at the region 400 nm to 800 nm.

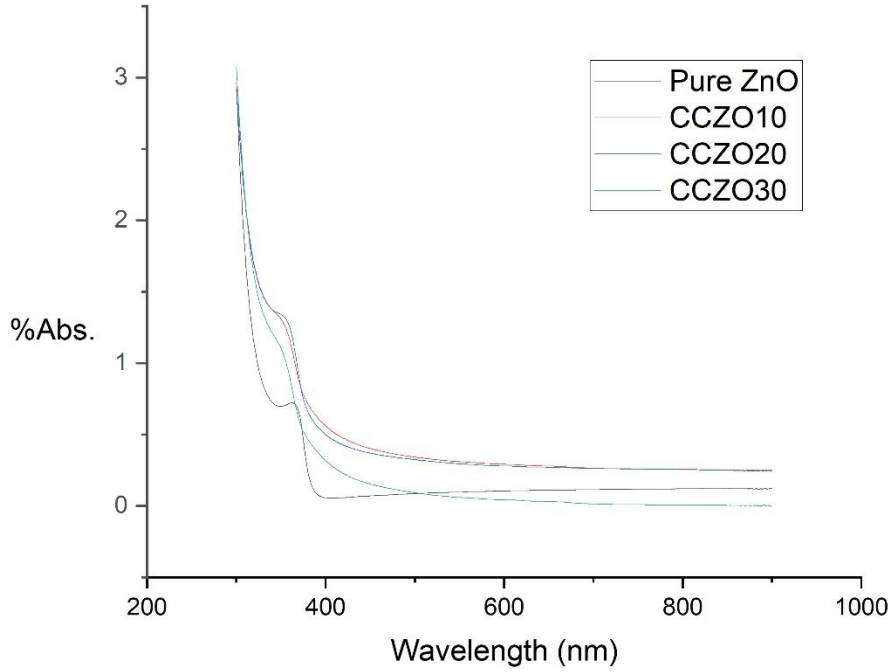

Figure 4.3: (b) UV-vis absorption spectrum of Pure ZnO, CCZO10, CCZO20 and CCZO30 films

A slight sharp absorption edge has been observed for undoped ZnO film. Noticeable gradually lower sharp edge for the doped zinc oxides respectively. Absorbance initially decreased sharply and then decreased gradually in all samples in visible range. The decrease in absorbance with doping may be attributed to the decrease of the size of the nanoparticles which ultimately widens the band gap. A sharp absorption edge is observed for pure ZnO. Shifting of the absorption edge towards the higher wavelength side around 380 to 400 nm is observed with increasing the doping percentage. These changes suggest with an increase in doping concentration, the band gap of ZnO film widens. Initially absorption decreased sharply and then a gradually decreased is observed in visible range. Because nanoparticles get smaller with doping, the bandgap eventually increases, which may be the cause of the drop in absorbance.[59]

The optical band gap (Eg) for the deposited films was calculated on the basis of spectral absorption for ZnO tupe direct band gap material using the Tauc's relation:

$$\alpha h\upsilon = A\,(h\upsilon - E_g)^{1/2} \ldots \ldots \ldots \ldots (4.3)$$

The band gap has been calculated by extrapolating the linear region of the plots ($\alpha h\upsilon$) 2 versus hυ on the energy axis as shown in Figure 6.10 (a-d).

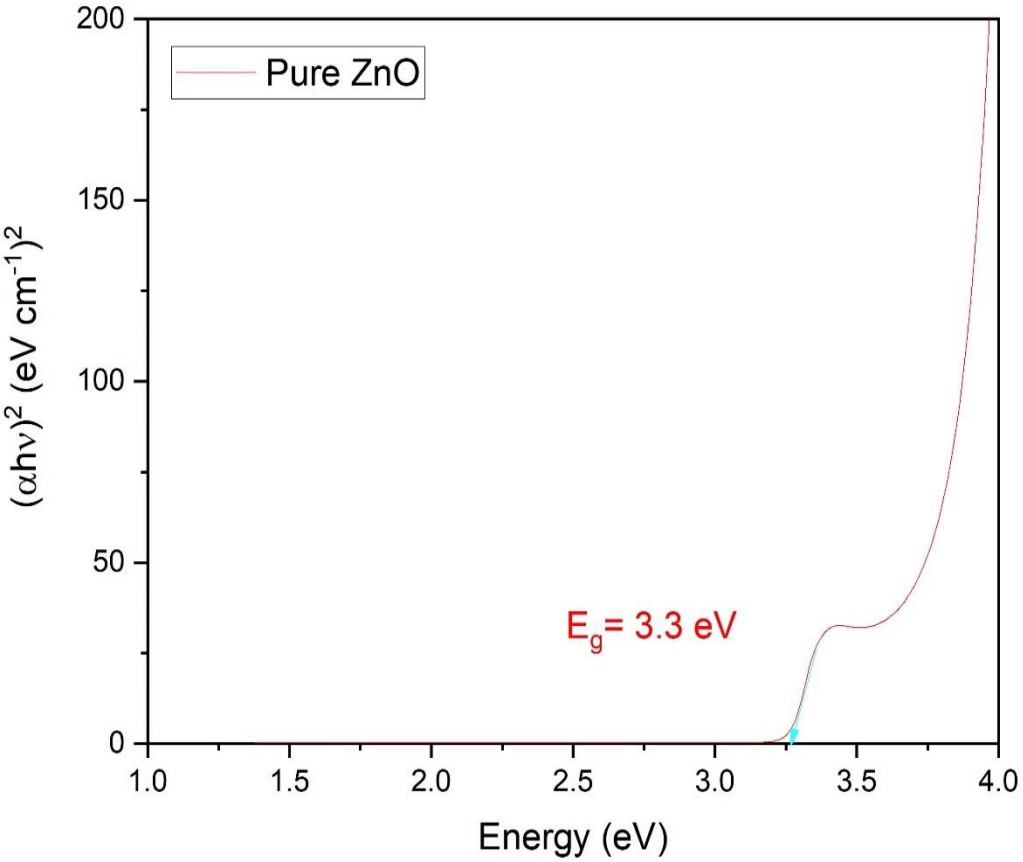

Figure (a)

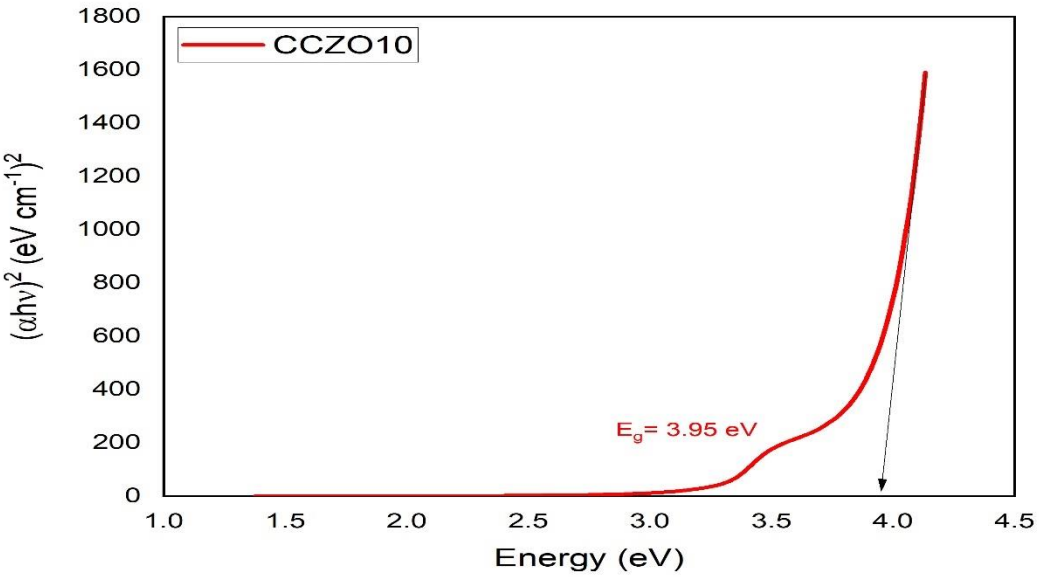

Figure (b)

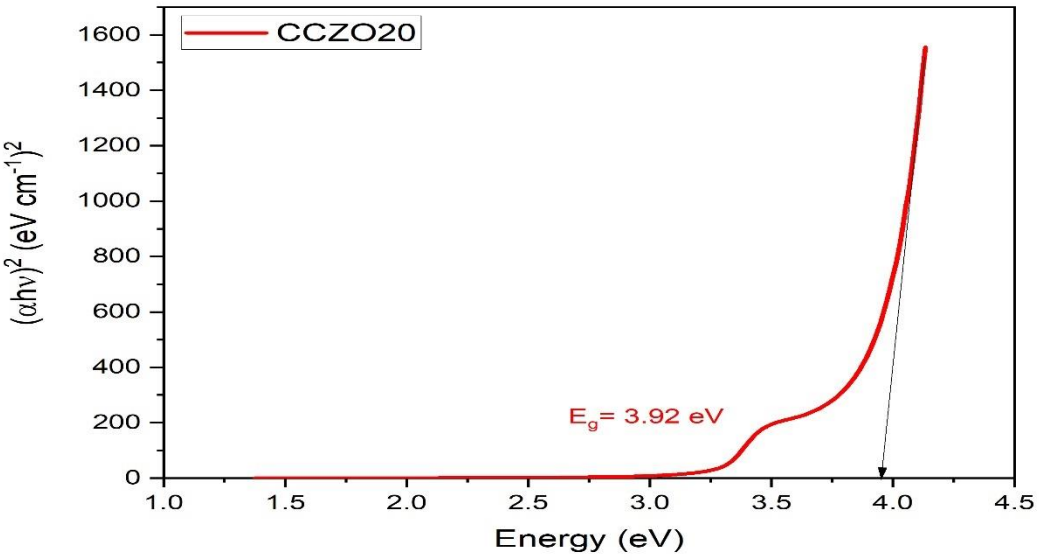

Figure (c)

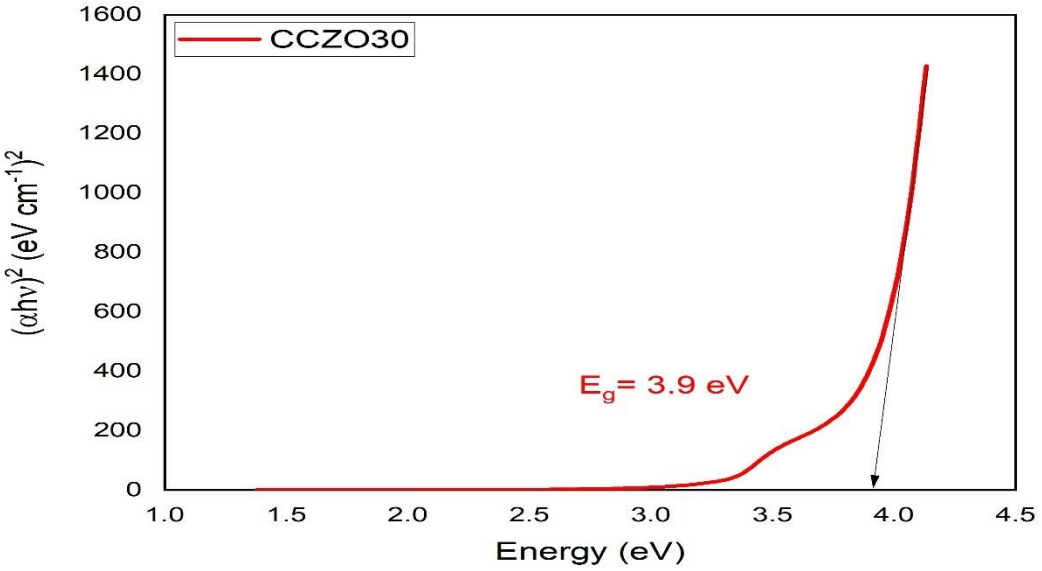

Figure (d)

Figure 4.4: Plot of $(\alpha h\upsilon)^2$ versus incident photon energy ($h\upsilon$) for (a) Pure ZnO, (b) CCZO10, (c) CCZO20 and (d) CCZO30 films

When compared to pure ZnO, the optical band gap for CCZO10, CCZO20, and CCZO30 films dramatically increased (Eg = 3.95, 3.92, and 3.9 eV, respectively) (3.3 eV). When the optical band gap widened with multiple elements doping, the concentration of n type carriers in the ZnO structure increased. [60,61,62]

By increasing the concentration of n type carriers through doping, the band gap is widened and the absorption edge occurs at considerably shorter wavelengths than in intrinsic materials. This is the well-known as Burstein–Moss effect.

CHAPTER V

CONCLUSION & RECOMMENDATIONS

5.1 Conclusion

The intended purpose of this study was to use a low-cost, simple sol-gel spin coating approach to evaluate the impacts of five elements doping (Cu, Co, Mn, Mg, and Ni) in ZnO wurtzite structure.

First of all, it was found that the manually operated, straightforward, and reasonably priced spin coating method was successful in depositing both pure ZnO and ZnO films that had been doped with Cu, Co, Mn, Mg, and Ni. In spite of the crystalline structure exhibiting increased disorder due to multi-element doping, therefore choosing an efficient and easy synthesis process was essential to go forward with the work. Spin coating is an ideal approach for film deposition to tackle this difficulty since the thin film is created from a precursor solution that is totally dissolved (every solute dissolves completely in the solvent).

In this study, as was previously said, thin films' structure and properties are influenced by a number of factors, including spinning speed, solution concentration, the glass substrates, and solution volume, among others. Therefore, altering the parameters used in this work would undoubtedly have an impact on how the structural, morphological and optical properties of formed films are characterized. Additionally, annealing as-deposited films at various temperatures and for varying lengths of time may significantly alter the film's characteristics.

Following the adjustment of the process conditions, deposited films were examined to determine whether or not they could keep the wurtzite structured single phase in the absence of any other phases. The thin films of all samples had exclusively wurtzite structured ZnO phase, according to a thorough structural analysis of the deposited materials. Then, more basic optical characterizations were carried out. The study's key conclusions can be summarized as follows.

(i) The entropic effect of multi-element doping in ZnO was investigated, and it can be said that larger multi-element doping entropy production can be a driving force in the case of high concentration doping in ZnO wurtzite phase.

(ii) Decreased crystallinity was found in CCZO10, CCZO20 and CCZO30 compared with pure ZnO films from XRD results.

(iii) Doped samples, particularly CCZO30 film, showed very good optical transparency, band gap widening, and improved optical conductivity. The increase in transmittance

was caused by doping's reduction in crystallite size and well-crystallinity than CCZO10 and CCZO20.

(iv) Due to improvements in optical transmittance, band gap widening with doping, this material may be a suitable candidate for use in LED, TCO, and other applications.

5.2 Recommendations

(i) Entropic contribution in the single phase structure stabilization ($Cu_xCo_xMn_xMg_xNi_x$) $Zn_{1-x}O$ where keeping x=0.01, 0.03, 0.05 can be investigated.

(ii) These type of other transitional metal oxide compounds can be explored to establish a new class of multi-doped entropy assisted ceramic oxides.

(iii) This work can be done and investigated characteristics with different annealing temperature.

(iv) Only 3d transition element doping can be used to continue this effort and find lower lattice distortion and higher magnetic characteristics.

CHAPTER VI

REFERENCES

[1] Jagadish, C., & Pearton, S. J. (Eds.). (2011). Zinc oxide bulk, thin films and nanostructures: processing, properties, and applications. Elsevier.

[2] Fortunato, E. M., Barquinha, P. M., Pimentel, A. C. M. B. G., Goncalves, A. M., Marques, A. J., Pereira, L. M., & Martins, R. F. (2005). Fully transparent ZnO thin-film transistor produced at room temperature. Advanced Materials, 17(5), 590-594.

[3] Kumar, R., Kumar, G., Al-Dossary, O., & Umar, A. (2015). ZnO nanostructured thin films: Depositions, properties and applications—A review. Materials Express, 5(1), 3-23.

[4] Yeh, J. W. (2013). Alloy design strategies and future trends in high-entropy alloys. Jom, 65(12), 1759-1771.

[5] Gludovatz, B., Hohenwarter, A., Catoor, D., Chang, E. H., George, E. P., & Ritchie, R. O. (2014). A fracture-resistant high-entropy alloy for cryogenic applications. Science, 345(6201), 1153-1158.

[6] Rost, C. M., Sachet, E., Borman, T., Moballegh, A., Dickey, E. C., Hou, D. ... & Maria, J. P. (2015). Entropy-stabilized oxides. Nature communications, 6, 8485.

[7] Callister, W. D., & Rethwisch, D. G. (2007). Materials science and engineering: an introduction (Vol. 7, pp. 665-715). New York: John Wiley & Sons.

[8] Streetman, B. G., & Banerjee, S. (1995). Solid state electronic devices (Vol. 4). Englewood Cliffs, NJ: Prentice Hall.

[9] Olsen, V. S. (2015). Synthesis and Characterization of Homoepitaxial ZnO Thin Films (Master's thesis).

[10] Liu, Y., Li, Y., & Zeng, H. (2013). ZnO-based transparent conductive thin films: doping, performance, and processing. Journal of Nanomaterials, 2013.

[11] Exarhos, G. J., & Zhou, X. D. (2007). Discovery-based design of transparent conducting oxide films. Thin solid films, 515(18), 7025-7052.

[12] Ayouchi, R., Leinen, D., Martın, F., Gabas, M., Dalchiele, E., & Ramos-Barrado, J. R. (2003). Preparation and characterization of transparent ZnO thin films obtained by spray pyrolysis. Thin Solid Films, 426(1-2), 68-77.

[13] Hartnagel, H., Dawar, A. L., Jain, A. K., & Jagadish, C. (1995). Semiconducting transparent thin films (p. 181). Bristol: Institute of Physics.

[14] Xu, D., Deng, Z., Xu, Y., Xiao, J., Liang, C., Pei, Z., & Sun, C. (2005). An anode with aluminum doped on zinc oxide thin films for organic light emitting devices. Physics Letters A, 346(1-3), 148-152.

[15] Minami, T. (2008). Substitution of transparent conducting oxide thin films for indium tin oxide transparent electrode applications. Thin solid films, 516(7), 1314-1321.

[16] H. Zeng, S. Yang, and W. Cai, "Reshaping formation and luminescence evolution of ZnO quantum dots by laser-induced fragmentation in liquid," Journal of Physical Chemistry C, vol. 115, no. 12, pp. 5038–5043, 2011.

[17] Mizoguchi, H., Eng, H. W., & Woodward, P. M. (2004). Probing the electronic structures of ternary perovskite and pyrochlore oxides containing Sn4+ or Sb5+. Inorganic chemistry, 43(5), 1667-1680.

[18] Sadewasser, S., Glatzel, T., Rusu, M., Jäger-Waldau, A., & Lux-Steiner, M. C. (2002). High-resolution work function imaging of single grains of semiconductor surfaces. Applied Physics Letters, 80(16), 2979-2981.

[19] Minami, T. (2000). New n-type transparent conducting oxides. MRS bulletin, 25(8), 38- 44.

[20] Gordon, R. G. (2000). Criteria for choosing transparent conductors. MRS bulletin, 25(8), 52-57.

[21] Coutts, T. J., Young, D. L., Li, X., Mulligan, W. P., & Wu, X. (2000). Search for improved transparent conducting oxides: A fundamental investigation of CdO, Cd_2SnO_4, and Zn_2SnO_4. Journal of Vacuum Science & Technology A: Vacuum, Surfaces, and Films, 18(6), 2646-2660.

[22] H. Liu, V. Avrutin, N. Izyumskaya, Ü. Özgür, and H. Morkoc, "Transparent conducting oxides for electrode applications in light emitting and absorbing devices," Superlattices Microstruct, vol. 48, no. 5, pp. 458 – 484, 2010.

[23] S.-M. Park, T. Ikegami, and K. Ebihara, "Effect of substrate temperature on the properties of Ga-doped ZnO by pulsed laser deposition," Thin Solid Films, vol. 513, pp. 90–94, 2006.

[24] Sahu, D. R.; Lin, S.-Y.; Huang, J.-L. ZnO/Ag/ZnO Multilayer Films for the Application of a Very Low Resistance Transparent Electrode. Appl. Surf. Sci. 2006, 252, 7509–7514

[25] Sahu, D. R.; Huang, J.-L. High Quality Transparent Conductive ZnO/Ag/ZnO Multilayer Films Deposited at Room Temperature. Thin Solid Films 2006, 515, 876–879.

[26] Kao, K.-S.; Chang, S.-H.; Hsieh, P.-T.; Wang, C.-M.; Cheng, D.- L. Transparence and Electrical Properties of ZnO-Based Multilayer Electrode. Appl. Phys. A: Mater. Sci. Process. 2009, 96, 529–533.

[27] B. G. Streetman and S. K. Banerjee, Solid State Electronic Devices. Pearson Prentice Hall, 6 ed., 2006. 28. J. C. Fan, K. M. Sreekanth, Z. Xie, S. L. Chang, and K. V. Rao, "p-type ZnO materials: Theory, growth, properties and devices," Progress in Materials Science, vol. 58, no. 6, pp. 874 – 985, 2013.

[29] Sandeep, K. M., Bhat, S., & Dharmaprakash, S. M. (2017). Structural, optical, and LED characteristics of ZnO and Al doped ZnO thin films. Journal of Physics and Chemistry of Solids, 104, 36-44.

[30] Y. Lixin, X. Zheng, H. Yanbing, Z. Xiqing, W. Yongsheng, X. Xurong, The ultraviolet and blue luminescence properties of ZnO:Zn thin films, Chin. Sci. Bull. 46 (2001) 1223.

[31] Q. Shi, C. Wang, S. Li, Q. Wang, B. Zhang, W. Wang, J. Zhang, H. Zhu, Enhancing blue luminescence from Ce-doped ZnO nanophosphor by Li doping, Nanoscale Res. Lett. 9 (2014) 480.

[32] S. Chawla, K. Jayanthi, H. Chander, Enhancement of luminescence in ZnMgO thin-film nanophosphors and application for white light generation, Phys. Status Solidi Appl. Mater. Sci. 205 (2008) 271

[33] R. B. Heller, J. McGannon, and A. H. Weber, "Precision determination of the lattice constants of zinc oxide," J. Appl. Phys., vol. 21, no. 12, pp. 1283–1284, 1950.

[34] Ü. Özgür, Y. I. Alivov, C. Liu, A. Teke, M. A. Reshchikov, S. Dogan, V. Avrutin, S. J. Cho, and H. Morkoc, "A comprehensive review of ZnO materials and devices," J. Appl. Phys., vol. 98, 2005.

[35] K. Momma and F. Izumi, “VESTA 3 for three-dimensional visualization of crystal, volumetric and morphology data,” J. Appl. Crystal logr., vol. 44, pp. 1272–1276, Dec 2011.

[36] Schmidt-Mende, L., & MacManus-Driscoll, J. L. (2007). ZnO–nanostructures, defects, and devices. Materials today, 10(5), 40-48.

[37] Han, J., Mantas, P. Q., & Senos, A. M. R. (2002). Defect chemistry and electrical characteristics of undoped and Mn-doped ZnO. Journal of the European Ceramic Society, 22(1), 49-59.

[38] Minami, T., Sato, H., Nanto, H., & Takata, S. (1985). Group III impurity doped zinc oxide thin films prepared by RF magnetron sputtering. Japanese journal of applied physics, 24(10A), L781.

[39] Yamamoto, T., & Katayama-Yoshida, H. (2001). Physics and control of valence states in ZnO by codoping method. Physica B: Condensed Matter, 302, 155-162.

[40] Maissel, L. I., Glang, R., “Handbook of Thin Film Technology” Mc. Graw-Hill Company, 1970.

[41] Schuegraf, K. K. (1988). Handbook of thin-film deposition processes and techniques: principles, methods, equipment, and applications. Noyes Data Corporation/Noyes Publications.

[42] J. B. Nehmann, N. Ehrmann, R. Reineke-Koch, and D. W. Bahnemann, “Aluminum-doped zinc oxide sol-gel thin films: Influence of the sol’s water content on the resistivity,” *Thin Solid Films*, vol. 556, Apr. 2014.

[43] M. J. Alam and D. C. Cameron, “Preparation and properties of transparent conductive aluminum-doped zinc oxide thin films by solgel process,” *Journal of Vacuum Science & Technology A*, vol. 19, pp. 1642–1646, July 2001.

[44] J. Gild, Y. Zhang, T. Harrington, S. Jiang, T. Hu, M.C. Quinn, W.M. Mellor, N. Zhou, K. Vecchio, J. Luo, High-Entropy metal diborides: a new class of high-entropy materials and a new type of ultrahigh temperature ceramics, Sci. Rep. 6 (2016) 37946,

[45] S. Jiang, T. Hu, J. Gild, N. Zhou, J. Nie, M. Qin, T. Harrington, K. Vecchio, J. Luo, A new class of high-entropy perovskite oxides, Scr. Mater. 142 (2018) 116 –120

[46] Ye, Y. F., Wang, Q., Lu, J., Liu, C. T., & Yang, Y. (2016). High-entropy alloy: challenges and prospects. Materials Today, 19(6), 349-362.

[47] Cullity, B. D., 'Elements of X-ray Diffraction' Addison-Wesley Publishing Company. Inc. USA, 1959.

[48] Kodom, K. (2011). Heavy metal pollution in soils from anthropogenic activities. LAP LAMBERT Academic Publishing, 120.

[49] C. H. Seager and S. M. Myers, J. Appl. Phys., 94, 2888–2894, Quantitative comparisons of dissolved hydrogen density and the electrical and optical properties of ZnO (2003).

[50] Zhu, F. Y., Wang, Q. Q., Zhang, X. S., Hu, W., Zhao, X., & Zhang, H. X. (2014). 3D nanostructure reconstruction based on the SEM imaging principle, and applications. Nanotechnology, 25(18), 185705.

[51] Shinde, V. R., Gujar, T. P., Lokhande, C. D., Mane, R. S., & Han, S. H. (2006). Mn doped and undoped ZnO films: A comparative structural, optical and electrical properties study. Materials Chemistry and Physics, 96(2-3), 326-330.

[52] https://www2.chemistry.msu.edu/faculty/reusch/virttxtjml/spectrpy/uv-vis/uvspec.htm

[53] Service Detail. (2019). Retrieved from http://14.139.58.69/icar_teldir/services/home/service_detail?name_instru=FTIR%20Spectrophotometer%20&unique_num=150&xdidz=361&p=../institute/instrument_image&d=services_inti&c=services_chargeinti&xdybz=institute_committee&qptsu=../institute/committee_image

[54] Etape, E. P., Foba-Tendo, J., Ngolui, L. J., Namondo, B. V., Yollande, F. C., & Nguimezong, M. B. N. (2018). Structural Characterization and Magnetic Properties of Undoped and Ti-Doped ZnO Nanoparticles Prepared by Modified Oxalate Route. Journal of Nanomaterials, 2018.

[55] Yousefi, R., Zak, A. K., & Jamali-Sheini, F. (2013). Growth, X-ray peak broadening studies, and optical properties of Mg-doped ZnO nanoparticles. Materials Science in Semiconductor Processing, 16(3), 771-777.

[56] Mahmood, K., & Park, S. B. (2013). Atmospheric pressure based electrostatic spray deposition of transparent conductive ZnO and Al-doped ZnO (AZO) thin films: effects of Al doping and annealing treatment. Electronic Materials Letters, 9(2), 161-170.

[57] V. P. Deshpande, S. D. Sartale, A. N. Vyas, A. U. Ubale, Temperature Dependent Properties of Spray Deposited Nanostructured ZnO Thin Films, International Journal of Materials and Chemistry, Vol. 7 No. 2, 2017, pp. 36-46

[58] Reddy, N. N. K., Akkera, H. S., Sekhar, M. C., & Park, S. H. (2017). Zr-doped SnO 2 thin films synthesized by spray pyrolysis technique for barrier layers in solar cells. Applied Physics A, 123(12), 761.

[59] Rahdar, A. (2013). Effect of 2-mercaptoethanol as capping agent on ZnS nanoparticles: structural and optical characterization. Journal of Nanostructure in Chemistry, 3(1), 10.

[60] Moss, T. S. (1954). The interpretation of the properties of indium antimonide. Proceedings of the Physical Society. Section B, 67(10), 775.

[61] Sernelius, B. E., Berggren, K. F., Jin, Z. C., Hamberg, I., & Granqvist, C. G. (1988). Band-gap tailoring of ZnO by means of heavy Al doping. Physical Review B, 37(17), 10244.

[62] Mondal, S. B. S. R., Bhattacharyya, S. R., & Mitra, P. (2013). Effect of Al doping on microstructure and optical band gap of ZnO thin film synthesized by successive ion layer adsorption and reaction. Pramana, 80(2), 315-326.